RESEARCH ARTICLE

Integrated global analysis in spider-flowers illuminates features underlying the evolution and maintenance of C_4 photosynthesis

Wei Zhao[1,†], Jun Li[1,†], Xingchao Sun[1], Qiwei Zheng[1], Wei Hua[1,2,*] and Jun Liu[1,*]

[1] Key Laboratory of Biology and Genetic Improvement of Oil Crops, Ministry of Agriculture and Rural Affairs, Oil Crops Research Institute of the Chinese Academy of Agricultural Sciences, Wuhan 430062, China.

[2] Hubei Hongshan Laboratory, Wuhan 430070, China.

[†] Equally contributed.

*Correspondence: liujunocr@caas.cn (J.Liu); huawei@oilcrops.cn (W.H.)

Short title: *Gynandropsis gynandra* genome evolution

One-sentence summary: We present a high-quality chromosome-scale genome assembly for dicot C_4 model crop *Gynandropsis gynandra* and find an independent evolutionary trajectory from C_3 to C_4 photosynthesis in *Cleome* genus.

The authors responsible for distribution of materials integral to the findings presented in this article in accordance with the policy described in the Instructions for Authors (https://academic.oup.com/plcell/pages/General-Instructions) are: Jun Liu (liujunocr@caas.cn) and Wei Hua (huawei@oilcrops.cn).

ABSTRACT

The carbon concentrating mechanism—C_4 photosynthesis—represents a classic example of convergent evolution. While how this important trait originated and evolved remains largely enigmatic. Here we present a high-quality chromosome-scale annotated genome assembly of the spider-flower *Gynandropsis gynandra*, a valuable leafy vegetable crop and medicinal plant that has also been recognized as an emerging C_4 model species. Repetitive elements occupy up to 71.91% of its genome, and over half are LTR-RTs derived from recent bursts, contributing to genome size expansion. Strikingly, LTR-RT explosion also played a critical role in C_4 evolution by altering expression features of photosynthesis-associated genes via preferential insertion in promoters. Synteny analysis in the *Cleome* genus unveils that an independent species-specific whole-genome duplication in *G. gynandra*, which we name Gg-α, occurred after divergence from its close relative C_3 plant *Tarenaya hassleriana*. Integrated multi-omics profiling demonstrates that Gg-α, gene family expansion, recent LTR-RT amplification and more recent species-specific tandem duplication events have all facilitated the evolution of C_4 photosynthesis, revealing uniqueness of C_4 evolution in this lineage. Moreover, high leaf vein density and heat stress resilience are associated with shifted gene expression patterns. Altogether, this mode of C_3-to-C_4 transition yields new insights into evolutionary convergence of a complex plant trait.

Keywords: convergent evolution, reference genome, C_4 biology, model plant, *Gynandropsis gynandra*

INTRODUCTION

Photosynthesis is the basis of most life forms on the planet. C_4 photosynthesis represents a remarkable convergent innovation that results from a series of anatomical and biochemical modifications to the ancestral C_3 photosynthetic pathway, which together function to increase CO_2 concentration around the enzyme RuBisCO, thereby reducing photorespiration and enhancing photosynthetic efficiency (Schlüter and Weber, 2020). Most, if not all, C_4 species, which possess a distinctive leaf structure characterized by Kranz anatomy, are typically classified into three metabolic subtypes based on the enzymes used to decarboxylate C_4 acids in their bundle sheath cells (BSC): NADP-ME, NAD-ME and PEP-CK (Zhao et al., 2022; Furbank, 2011). C_4 plants usually have higher photosynthetic capacity and higher nitrogen and water-use efficiencies than their C_3 relatives and thus tend to be more productive (Sage, 2004; Sage et al., 2012). In particular, C_4 photosynthesis outperforms the ancestral C_3 state under sunny, hot and dry circumstances, which are projected to become more prevalent with global climate changes (Hibberd et al., 2008; Wang et al., 2021).

The introduction of dual-celled C_4 photosynthesis into C_3 plants is proposed to be a promising strategy to sustainably meet the rising food, fuel and feed demands worldwide (Wang et al., 2016; Ermakova et al., 2020). This goal requires a profound understanding of the origin, genetic architecture and developmental features of C_4 syndrome as compared to C_3. Several C_4 monocots, including maize (*Zea mays*), sorghum (*Sorghum bicolor*) and millets (*Setaria viridis* and *Setaria italica*), have been used as model plants for this purpose (Paterson et al., 2009; Mamidi et al., 2020; Bennetzen et al., 2012; Jiao et al., 2017). However, these models share various disadvantages including relatively large size, complex genomes, long life cycles and low transformability (Brown et al., 2005). Fortunately, a mini foxtail millet mutant, *xiaomi*, has recently been established as a new NADP-ME subtype C_4 model system (Yang et al., 2020). However, all current C_4 model plants are monocotyledonous species, and there are differences in C_4 attributes of dicots and monocots, including vein patterning, Kranz anatomy morphogenesis, regulation of C_4 photosynthetic enzymes and development of C_4 capacity (Ermakova et al., 2020; Schlüter and Weber, 2020). Therefore, it is vital to develop a dicot C_4 model plant and would furthermore be advantageous to develop a model system in NAD-ME or PEP-CK subtypes of C_4 plants. Investigation of these C_4 model organisms would accelerate systematic understanding of C_4 biology and facilitate synthetic engineering of the C_4 pathway into contemporary C_3 crops.

The dicot *Gynandropsis gynandra* (common names: spider-flower, African cabbage, bastard-mustard and cat's-whiskers) is an important traditional C_4 crop native to Asia and

Africa, currently cultivated around the world (Oshingi et al., 2019). The leaves and seeds of *G. gynandra* are rich in proteins, vitamins, minerals and other beneficial health compounds with antioxidant, anti-inflammatory and anti-microbial properties, and *G. gynandra* has thus been widely used as a leafy vegetable or medicinal plant (Moyo and Aremu, 2021). As a C_4 species, *G. gynandra* displays high photosynthetic efficiency and adaptation to severe environmental stresses such as high temperature, water deficit or high salinity (Sogbohossou et al., 2018). Importantly, it is a diploid crop characterized by relatively short life cycle, small size, simple growth requirements, prolific seed production, self-compatibility and autogamy. Besides, *G. gynandra* has a rich diverse germplasm that provides valuable genetic material for dissecting traits of interest and breeding (Sogbohossou et al., 2019). These advantages, coupled with its efficient genetic transformation system, make this plant an ideal model plant for C_4 biology (Newell et al., 2010).

G. gynandra belongs to family of Cleomaceae, the sister clade to Brassicaceae, and is phylogenetically closest to the dicot C_3 model plant *Arabidopsis thaliana*, enabling the utilization of molecular resources and tools developed for *Arabidopsis* in *G. gynandra* and facilitating knowledge transfer (Marshall et al., 2007; Koteyeva et al., 2011; Patchell et al., 2014; Hoang et al., 2022). Moreover, *G. gynandra*, together with the congeneric C_3 species *Tarenaya hassleriana* (common names: spider-flower, pinkqueen and grandfather's-whiskers), provides an invaluable genetic platform for comparative studies of many intriguing biological phenomena including the evolutionary trajectory and developmental progression from C_3 to C_4 (Bräutigam et al., 2011; Külahoglu et al., 2014; Bayat et al., 2018; Hüdig et al., 2022). However, there is no published reference genome for *G. gynandra*, which hinders its use for fundamental biological discovery, technological advances and applications for genetic engineering. To address this gap, we generated a high-quality chromosome-level reference genome assembly of *G. gynandra*, establishing it as a C_4 model system for dicotyledonous and NAD-ME subtype plants. Our comprehensive comparative genomic and transcriptomic analyses between *G. gynandra* and *T. hassleriana* using new and existing data not only help explain why C_4 photosynthesis failed to evolve in *T. hassleriana* but also demonstrate the flexibility of the convergent evolution of this ecologically important but complex trait. The availability of this reference-grade genomic resource, together with its amenability to genetic transformation, makes *G. gynandra* an ideal model system for understanding the unique C_4 biology and facilitating efforts toward C_4-aimed crop engineering.

RESULTS

Chromosome-scale assembly and annotation of *G. gynandra* genome

Based on *k*-mer analysis, the dicotyledonous C_4 plant *G. gynandra* (2n=2x=34) had an estimated genome size of approximately 997.61 Mb with low heterozygosity (0.13%) but high repetitive sequence content (79.72%) (Supplemental Figure S1 and Supplemental Data Set S1). To construct a reference-grade genome for *G. gynandra*, we employed an optimized strategy combining long-read Oxford Nanopore Technology (ONT), short-read Illumina sequencing and high-throughput chromatin conformation capture (Hi-C) for chromosome scaffolding (Supplemental Figure S2). A total of 144.37 Gb (~180 ×) of ONT long sequences with an N50 read length of 24.57 kb were generated (Supplemental Figure S3 and Supplemental Data Set S2). The ONT long reads were *de novo* assembled into contigs, followed by polishing with both ONT and Illumina reads. To further anchor and orient the contigs onto chromosomes, we prepared Hi-C libraries from young leaves to construct chromatin interaction maps, generating 130 Gb (~162 ×) paired-end reads (Supplemental Data Set S3). This resulted in a final assembly of 984.21 Mb comprising 109 scaffolds, which represented 98.66% of the estimated nuclear genome (Table 1 and Supplemental Data Set S4). The contig N50 and scaffold N50 were 11.43 Mb and 51.02 Mb, respectively. Sequences of 909.61 Mb covering 171 contigs were assigned to seventeen pseudo-chromosomes (Chr1–Chr17; Figure 1A and Table 1), which accounted for 92.42% of the assembly. The pseudo-chromosomes of *G. gynandra* ranged from 41.13 to 72.98 Mb in size (Supplemental Data Set S5). Of note, a 55.56 Mb contig, which covered 98.7% of the intact Chr5, constituted a near complete, telomere-to-telomere assembly of one *G. gynandra* chromosome.

The assembly quality of the *G. gynandra* genome was evaluated by multiple approaches. First, Hi-C interaction matrices for the constructed pseudo-chromosomes visualized as a Hi-C heatmap showed a clear anti-diagonal pattern for intra-chromosomal interactions (Figure 1B). Second, the completeness of assembly as analyzed with Benchmarking Universal Single Copy Orthologues (BUSCO) was 95.6% (Supplemental Data Set S6). Third, RNA-seq reads obtained from six representative tissues of flower bud, flower, leaf, root, stem and silique were mapped back onto *G. gynandra* genome, to which approximately 96.16–98.33% of the reads could be aligned (Supplemental Data Set S7). Finally, long terminal repeat (LTR) assembly index (LAI), a metric using intact LTRs to evaluate assembly continuity, has been particularly utilized to assess assembly quality of plant genomes with high repetitive sequence content (Ou et al., 2018). The LAI score of *G. gynandra* assembly was 16.46, higher even than that of the *A. thaliana* reference genome (LAI = 15.62). Collectively, these

148 data demonstrate that *G. gynandra* genome assembly is of high quality in contiguity,
149 completeness and accuracy.

150 By integrating *ab initio*-based prediction, protein homology-based prediction and RNA-
151 seq/Iso-Seq data, we annotated a total of 34,772 protein-coding genes spanning 119.12 Mb
152 regions, representing 12.1% of the *G. gynandra* genome (Table 1). The gene density
153 distribution along each chromosome was uneven, with higher gene density towards the ends
154 of chromosome arms (Figure 1A). The total number of identified transcripts (including
155 splicing variants) was 41,843. Functional analysis predicted 33,100 (95.19%) genes with
156 known functional annotations in public databases, suggesting highly reliable gene prediction
157 (Supplemental Data Set S8). Moreover, we identified 2,359 non-coding RNAs including 120
158 miRNAs, 1,153 tRNAs and 1,086 rRNAs (Supplemental Data Set S9), and also 2,178
159 transcription factors (Supplemental Data Set S10). Of all the protein-coding genes, 95.9%
160 was assigned to 13,918 gene families in *G. gynandra*, which was comparable to *T.*
161 *hassleriana* (97.8% to 14,044 gene families). However, the former had an average of 2.39
162 genes per family, with the latter possessing 1.91 (Supplemental Data Set S11). Compared
163 with *A. thaliana*, *B. rapa*, *B. oleracea* and *T. hassleriana,* 1,051 gene families containing
164 6,517 genes were specific to *G. gynandra* (Figure 1C). These unique genes were primarily
165 enriched in metabolic pathways such as biosynthesis of amino acids, carbohydrates, lipids,
166 cofactors and vitamins, terpenoids and polyketides, which is consistent with the nutraceutical
167 food and ethnopharmacological medicinal uses for *G. gynandra* (Supplemental Figure S4).

168 Phylogenetic analysis was performed based on 661 single-copy orthologous genes among
169 ten angiosperm species including eight dicots (*A. thaliana*, *Brassica oleracea*, *Brassica rapa*,
170 *G. gynandra*, *T. hassleriana*, *Gossypium raimondii*, *Medicago Sativa* and *Solanum*
171 *lycopersicum*) and two monocots (*Oryza sativa* and *Z. mays*). The results revealed that *G.*
172 *gynandra* was the most closely related to *T. hassleriana*, both of which were adjacent to *A.*
173 *thaliana* (Figure 1D). Using a reference divergence times of *B. oleracea–B. rapa*, *Z. mays–O.*
174 *sativa* and *A. thaliana–O. sativa* obtained from the TimeTree database, the divergence
175 between Cleomaceae and Brassicaceae was estimated as 51.2 million years ago (MYA), with
176 C_4 *G. gynandra* and C_3 *T. hassleriana* sharing a common ancestor approximately 33.6 MYA.
177 Remarkably, the genome size of *G. gynandra* (984.21 Mb) is nearly fourfold as large as *T.*
178 *hassleriana* (249.93 Mb).

179

180 **Recent bursts of transposons massively bloated the *G. gynandra* genome, and LTR-RTs**
181 **facilitated the evolution of C_4 photosynthesis**

182 By combining *de novo*- and homology-based repeat family identification approaches, we
183 annotated a total of 707.8 Mb repetitive sequences, representing 71.91% of the *G. gynandra*
184 genome (Table 1). 613.5 Mb of sequences (62.33% of the total assembly) were classified as
185 transposable elements (TEs), including 485.73 Mb (79.17% of TEs) of LTR retrotransposons
186 (LTR-RTs) and 118.88 Mb of DNA transposons, whereas their size and proportion were
187 dramatically lower in *T. hassleriana* (Figure 2A and Supplemental Data Set S12). The spatial
188 distribution of LTR-RTs along chromosomes of *G. gynandra* was uneven (Supplemental
189 Figure S5). Its genome was found containing a considerable number of intact LTR-RTs with
190 sequence length up to 10,000 bp, with a peak at around 7,500 bp, while the peak in *T.*
191 *hassleriana* occurred at approximately 5,000 bp (Figure 2B). Most (79.72%) intact LTR-RT
192 insertion events in *G. gynandra* genome occurred within 1 MYA, with the peak of
193 amplification occurring around 0.16 MYA, in contrast to approximately 0.31 MYA for *T.*
194 *hassleriana* (Figure 2C). At the superfamily level, very recent amplifications of *Gypsy*
195 retrotransposons occurred approximately 0.14 MYA in *G. gynandra* (Figure 2D). *Gypsy*
196 retrotransposons had the highest distribution density in the centromeric area and the lowest
197 toward telomeric regions, with *Copia* showing a continuous distribution pattern (Figure 1A).
198 Recent massive expansion of LTR-RTs led us to explore their biological relevance. There
199 were 20,094 homologous gene pairs in total between the genomes of *G. gynandra* and *T.*
200 *hassleriana*. Relative to homologues without LTR-RTs, their presence caused more to be up-
201 regulated (Supplemental Figure S6A). LTR-RTs were found to reside preferentially within
202 promoter regions of protein-coding genes, especially in *G. gynandra* (Supplemental Figure
203 S6B), potentiating their differential roles in regulating gene expressions between the two
204 *Cleome* species. More than 70% of *G. gynandra* genes had LTR-RT insertions in their
205 promoter regions, which were only 23% for *T. hassleriana* (Figure 2E). Functional
206 enrichment analysis of these preferentially inserted genes indicated that pathways of
207 development, cell cycle, transcription regulation, redox regulation, stress-related, glycolysis,
208 Calvin cycle, photorespiration and light reaction were over-represented in *G. gynandra*
209 compared with *T. hassleriana* (Figure 2F). Furthermore, we identified 6,283 genes in *G.*
210 *gynandra* whose promoter regions contained substantially more LTR-RT insertions than their
211 orthologs in *T. hassleriana* (Supplemental Data Set S13). To assess the consequence of LTR-
212 RT amplification in these genes, their expression levels were analyzed in *G. gynandra*
213 relative to *T. hassleriana*. Moreover, we found that the proportions of genes with up-
214 regulated expression were much greater than those of down-regulated across the six
215 developmental stages, being more pronounced at the early stages (Figure 2G). Notably, the

216 significantly up-regulated genes along the development gradients included a subset of genes
217 associated with C_4 metabolism (Figure 2H), such as C_4 cycle (*NAD-MDH*, *NADP-ME1*,
218 *NADAP-MDH*, *PEP-CK*, *NHD1*, *ALAAT2* and *ASPAT*), light-harvesting complex (*LhcA3*),
219 photosystem (*PasG* and *PsbQ-2*), cyclic electron flow (CEF, *PnsB3* and *PGR5*), Calvin cycle
220 (*FAB6* and *TIM*), redox regulation (*GPX6* and *NTRB*), N assimilation (*NodGS* and *NIR1*),
221 auxin signaling (*SAUR35* and *PIN6*), vein venation (*SCR*, *TMO6* and *ANT*), as well as heat
222 stress response (*HSP81.2* and *HSP21.7*). In contrast, photorespiration genes with more LTR-
223 RTs (*BASS*, *DIC2* and *DiT*) were severely down-regulated in *G. gynandra*. Additionally,
224 LTR-RT insertions caused few C_4 metabolism-related genes to be down-regulated as well,
225 such as the copies of *NAD-MDH* (*GG09G088650* and *GG12G084140*), *NADP-ME*
226 (*GG11G010180*) and *PEPC* (*GG02G076930*) (Supplemental Figure S6C). Intriguingly,
227 several C_4 cycle genes whose promoter regions had less LTR-RTs in *G. gynandra* than in *T.*
228 *hassleriana* showed much higher levels of expression, such as *NAD-ME* homologues
229 (*GG09G104820* and *GG02G000360*) and *PPDK*. Together, these data reveal that recent
230 large-scale TE bursts are the driving force behind genome size expansion and that LTR-RTs
231 also play a role in the C_4 evolution of *G. gynandra*.
232
233 **Evidence for species-specific whole-genome duplication and tandem gene duplication**
234 **events in *G. gynandra***
235 A paleopolyploidization event has been reported for the *Cleome* genus, and *T. hassleriana*
236 underwent a whole-genome triplication (WGT) (Cheng et al., 2013; van den Bergh et al.,
237 2014). However, it remains to clarify whether this event is specific to *T. hassleriana* or
238 shared with *G. gynandra*. We thus analyzed syntenic blocks within the *G. gynandra* genome
239 through intra-genome comparisons, identifying 771 syntenic blocks with 8,801 paralogous
240 gene pairs (Supplemental Data Set S14). We detected multiple duplications in *G. gynandra*
241 based on synteny, with many pairs of paralogous genes. Specifically, chromosomes Chr1,
242 Chr2, Ch3, Chr4, Chr7, Chr10 and Chr14 corresponded closely with Chr8, Chr6, Chr5, Chr12,
243 Chr11, Chr15 and Chr16, respectively (Figures 1A and 3A). Additionally, intra-chromosomal
244 rearrangements, especially inversions, were pervasive in *G. gynandra* such as those near the
245 arm ends of Chr10 and Chr15. Collinearity analysis also showed that chromosome Chr9 and
246 Chr6 shared syntenic regions with Chr2. Likewise, chromosome Chr17 and Chr8 shared
247 syntenic regions with Chr1, and Chr5 was collinear with both Chr3 and Chr13. Overall, these
248 chromosomes displayed high levels of structural variations, suggesting existence of
249 considerable chromosome rearrangements in *G. gynandra*.

250 For inter-species comparison, we examined genomic synteny between *G. gynandra* and *A.*
251 *thaliana* and *V. vinifera* chromosomes, resulting in a 2-to-2 syntenic relationship with *A.*
252 *thaliana*, and 4-to-1 with *V. vinifera* (Figure 3B and Supplemental Figure S7, A and B). Of
253 note, synteny analysis between *G. gynandra* and *T. hassleriana* showed a 2-to-3 syntenic
254 relationship (Supplemental Figure S7C). Given that *V. vinifera* has not undergone genome
255 duplication (Jaillon et al., 2007), and that *A. thaliana* experienced a recent whole-genome
256 duplication (WGD, termed At-α) (Jiao et al., 2011), we thus named the species-specific WGD
257 event in *G. gynandra* and WGT event in *T. hassleriana* Gg-α and Th-α, respectively. To
258 further infer the time of this Gg-α, we calculated the density distribution of K_s (synonymous
259 substitution rate) and D4DTv (distance of fourfold degenerate transversion) values of
260 collinear gene pairs within *G. gynandra*, *T. hassleriana, A. thaliana* and *B. rapa*. The
261 distribution of K_s values showed that *G. gynandra* had one main peak at K_s of ~0.475 (~22
262 MYA), which was slightly earlier than *B. rapa* at ~0.313 (~14.7 MYA) and *T. hassleriana* at
263 ~0.390 (~18.4 MYA), and later than *A. thaliana* at ~0.737 (~35 MYA; Figure 3, C and D).
264 The distribution of D4DTv in these four species corroborated time relationships of the WGD
265 or WGT event (Supplemental Figure S7D). About 85.5% of genes in *G. gynandra* genome
266 were duplicated and retained from WGD, which was much higher than the proportion of
267 63.5% for *T. hassleriana* (Figure 3E). Functional enrichment analysis of these WGD/WGT-
268 derived genes identified pathways such as photosynthesis, ATP synthesis and stress responses
269 as markedly enriched in *G. gynandra* relative to *T. hassleriana* (Supplemental Figure S8A).
270 In addition to WGD, we also identified 610 tandem duplicated genes (TDGs), which were
271 involved in various pathways (Figure 3F). Of importance, the carbon fixation pathway in
272 photosynthetic organisms was exceptionally enriched among *G. gynandra* TDGs, with five
273 duplicated genes including *PEPC2*, *NAD-MDH*/*mMDH1*, *GAPC1* and *PDE345*. Their K_s
274 values were all less than 0.1, indicating that these TDGs derived from the very recent
275 duplications after Gg-α (Figure 3G). Except for *PDE345*, the other TDGs exhibited dynamic
276 expression levels from young to mature leaves of *G. gynandra* (Supplemental Figure S8, B
277 and C). Collectively, these results revealed that unlike C_3 *T. hassleriana*, *G. gynandra*
278 experienced species-specific WGD (Gg-α) and tandem duplication events, both of which
279 likely facilitated C_4 photosynthesis evolution.
280
281 **Expanded gene families have contributed to C_4 trait formation**
282 Closer inspection of gain and loss within gene families showed that 978 and 1,449 ones have
283 undergone expansion and contraction in *G. gynandra*, respectively (Figure 4A). Pfam

284 annotation showed that the genes of expanded families contained protein kinase domain,
285 RING finger, DnaJ domain, PPR repeat, NAD dependent epimerase/dehydratase family,
286 NAD(P)H-binding and AP2 domain (Supplemental Data Set S15). Notably, we identified 221
287 expanded orthogroups, which were shared by the C_4 dicot *G. gynandra* and C_4 monocot *Z.*
288 *mays* (Figure 4B). These commonly enriched families could be mainly classified into six
289 functional categories: hormone response/signal transduction, gene transcription/protein
290 homeostasis, cell development, leaf development, photosynthetic performance and stress
291 resilience (Figure 4C and Supplemental Figure S9). Specifically, the hormone response/signal
292 transduction category contained a number of genes involved in metabolic processes of auxin,
293 abscisic acid, ethylene or cytokinin, and light signal conduction. Many of these genes also
294 participated in gene transcription/translation or protein homeostasis. Particularly, genes
295 associated with cell and leaf developments were expanded in both C_4 species, such as cell
296 cycle, programmed cell death, vascular bundles development, chloroplast biogenesis and
297 photomorphogenesis. Expansion of genes in light and in dark reactions could enhance
298 photosynthetic efficiency of C_4 plants, and gene families involved in resistance to abiotic or
299 biotic stress were also expanded (Figure 4C). These results suggest that the fitness advantages
300 of C_4 species may have relevance to expansions of defined gene families.
301
302 **Gene expression patterns for high vein density and heat stress tolerance associated with**
303 **maitenence of C_4 photosynthesis in *G. gynandra***
304 The fitness advantages of C_4 species are typically linked to alerations in leaf vein density or
305 stress resistence during evolution. *G. gynandra* and *T. hassleriana* exhibited similar
306 phenotypes regarding the morphology and leaf development (Figure 5A). However, *G.*
307 *gynandra* possessed evidently denser veins (Figure 5B) and typical Kranz anatomy compared
308 to *T. hassleriana* (Supplemental Figure S10). To identify potential discrepant features
309 between these dicotyledonous C_3 and C_4 plants, their leaf samples from five developmental
310 stages were collected under normal and heat stress conditions (Supplemental Figure S11). We
311 found that *G. gynandra* had significantly higher vein density than *T. hassleriana* during early
312 (S1), middle (S3) and mature (S5) stages (Figure 5C). Many of the well-known genes
313 encoding vasculature developmental factors had differential expression patterns between the
314 two species (Supplemental Figure S12). To dissect mechanisms underlying the differences in
315 transcriptional regulation of the leaf vasculature, we constructed large-scale gene regulatory
316 networks (GRN) based on RNA-seq time series datasets of *G. gynandra* and *T. hassleriana*
317 using GENIE3, and candidate target genes of TFs were then predicted (Supplemental Figure

318 S13). Among many of the TFs, the *Dof* family is established to be enriched in BSC and bind
319 to AAAG motifs (Dai et al., 2022). Twenty-one and twenty-four hub genes from *Dof*-GRNs
320 were identified for *G. gynandra* and *T. hassleriana*, respectively (Figure 5D). In addition to
321 the well-documented *Dof* genes with important roles in vein development, such as *CDF2*,
322 *CDF3*, *OBP2*, *OBP4*, *PEAR2*, *Dof2.4*, *HCA2* and *TMO6*, we also found some *Dof* genes with
323 unknown functions, including *Vdof1*, *Dof1.4*, *Dof1.7*, *Dof1.8*, and *Dof2.2* (Supplemental Data
324 Set S16). By analyzing of the previously deposited cell-specific transcriptomic data (Aubry et
325 al., 2014), we found that both homologous genes of *Vdof1* in *G. gynandra* exhibited
326 preferential expressions in BS cells (Supplemental Figure S14). The potential target genes of
327 *G. gynandra Vdof1* were shown to be mainly enriched in pathways for chlorophyll
328 metabolism, photosynthesis, and RNA and protein metabolism (Figure 5E). Overexpression
329 of *Vdof1* conferred significantly higher photosynthetic efficiency, leaf vein density and heat
330 resistance in *Arabidopsis* plants, whereas its corresponding mutants displayed the opposite
331 effects (Supplemental Figure S15). Research on molecular mechanisms of *Vdof1* in
332 regulating these C_4 photosynthesis-associated processes is currently underway.
333 We further examined the response of *G. gynandra* and *T. hassleriana* plants to heat stress
334 treatment. Apparently, *G. gynandra* was much more tolerent to high teperature than *T.*
335 *hassleriana* (Figure 5F). We then analyzed differential gene expression in the two species. A
336 total of 16,138 and 18,492 differential expression genes (DEGs) were identified in *G.*
337 *gynandra* and *T. hassleriana*, respectively (Supplemental Data Set S17). The heat stress
338 response pathway was significantly up-regulated at all the stages in *G. gynandra* but not in *T.*
339 *hassleriana* (Supplemental Figure S16). A set of *Hsf*, *Hsp100*, *Hsp90*, *Hsp70*, *Hsp60* and
340 *sHsp* was identified in both species (Supplemental Data Set S18). However, 12–40% of *Hsf*
341 genes in *G. gynandra* exhibited significantly up-regulated expressions after heat treatments,
342 compared to 7–19% for *T. hassleriana*, depending on the leaf developmental stage (Figure
343 5G), and a larger number of *Hsp100*, *Hsp90*, *Hsp70*, and *Hsp60* genes were up-regulated in *G.*
344 *gynandra*. Consistently, the photosynthesis pathway was over-represented among the heat-
345 upregulated genes of *G. gynandra*, regardless of developmental stage (Supplemental Figure
346 S16). The expression levels of a subset of C_4 metablism-related genes were induced in *G.*
347 *gynandra* under heat stress, such as *CA* (*GG03G120380*), *NAD-MDH* (*GG12G084140* and
348 *GG09G089650*), *PEPC* copies, *PPDK*, *ALAAT* (*GG06G105780*), *ASPAT* (*GG07G009900*)
349 and *NHD* copies, as were N assimilation pathway genes including *GS2* and *NiR* copies
350 (Supplemental Figure S17). Carbon fixation, S assimilation and redox regulation pathways
351 were largely unaffected, except for several *TPT* copies being up-regulated. While diffrential

352 expression patterns were observed for photorespriration pathway genes between *G. gynandra*
353 and *T. hassleriana*.
354
355 **Expression features and evolution of key genes involved in C_4 photosynthesis and**
356 **photorespiration**
357 An illustration for NAD-ME subtype of C_4 photosynthesis was shown (Figure 6A). Targeted
358 analysis of the copy number of C_4 cycle genes revealed that the ratio of gene copy number in
359 *G. gynandra* vs *T. hassleriana* was largely higher than 2:3, which is the baseline expected
360 ratio given their genomic relationship (Supplemental Figure S18). This suggests that *G.*
361 *gynandra* likely retained more C_4 genes after WGD, whereas *T. hassleriana* could have lost a
362 subset of these genes after WGT (Supplemental Data Set S18). For instance, there were six
363 copies of *NAD-MDH* in both species, nine and ten copies of *GAPDH* in *G. gynandra* and *T.*
364 *hassleriana*, respectively, and even more copies of *GOGAT* (4:2) and *GDCP* (3:2) were
365 found in *G. gynandra* compared to *T. hassleriana* (Supplemental Data Set S18). Furthermore,
366 all the enzymes characterizing NAD-ME subtype were identified in *G. gynandra* (Figure 6B
367 and Supplemental Data Set S18), and their gene expression in six different tissues were
368 assessed. Transcript levels of the main candidate *NAD-ME* (*GG02G000360*) and *NAD-MDH*
369 (*GG02G075940*) genes were over 1,406-fold and 7-fold higher in leaves than roots,
370 respectively, whereas all the candidate *NADP-ME* and *PEP-CK* genes had drastically
371 decreased expressions in leaves than in the other tissues. The expression levels of *Dit*, *NHD*,
372 *BASS*, *TPT* and *AlaAT* genes were highest in leaves. These results indicate that C_4 enzyme
373 genes are preferentially expressed in photosynthetic tissues and that *G. gynandra* performs
374 the NAD-ME subtype of carbon fixation. Futhermore, candidate homologous enzymes
375 involved in C_4 carbon fixation in *G. gynandra* were identified based on their preferential
376 expression in photosynthetic tissues and phylogenetic analysis with known C_4 genes
377 (Supplemental Figure S19), which could be NAD-ME2 (GG02G000360), NAD-
378 MDH/mMDH1 (GG02G075940 and GG02G075810), PEPC2 (GG14G004940,
379 GG14G005080 and GG14G005010), PEPC-K/PPCK1 (GG05G088230), PPDK
380 (GG13G000810), PPDK-RP/RP1 (GG12G002660), CA1 (GG15G098730 and
381 GG10G000490) and CA4 (GG17G084960), ASPAT/ASP5 (GG07G010040), and ALAAT2
382 (GG06G105780).
383 The restriction of Gly decarboxylase (GDC) to BSC results in formation of the
384 photorespiratory CO_2 pump that is an essential step during C_3-to-C_4 transition. This promoted
385 us to examine how P-protein of GDC (GDCP) and its promoter elements are altered in C_3, C_4

386 dicot and C_4 monocot species (Figure 6C). Interestingly, three copies of *GDCP* gene were
387 detected in *G. gynandra*, while a single copy was present in C_4 monocots (*S. bicolor*,
388 *Sorghum italica* and *Z. mays*) and 1–2 copies were in C_3 plants. A total of seven conserved
389 motifs (motif 1 to 7) were identified in promoter regions of these *GDCP* genes. Motif 1
390 containes an element (M-box) that has reported to drive expression in mesophyll cells (MC),
391 with motif 6 harboring a regulatory element (V-box) being required for vasculature
392 expression (Adwy et al., 2015, 2019). Unexpectedly, M-box, but rather V-box, was present in
393 the promoters of two *GDCP* genes (*GG08G031990* and *GG07G022890*) in *G. gynandra*, and
394 no known motifs could be detected in the other one *GG11G095250*. It should be metioned
395 that neither M-box nor V-box was found in the *GDCP* of C_4 monocots. Notably, a single
396 *GDCP* (*GG08G031990*) was the most abundantly expressed in *G. gynandra*, with the highest
397 levels in leaf tissue, while the other two duplicates were expressed at extremely low levels in
398 all tissues analyzed (Figure 6D). This paralog was uniquely increased along leaf
399 developmental gradients and could be further dramatically induced by heat stress (Figure 6E).
400 Based on our data, we proposed a hypothetical model for the evolution and maintenance of
401 C_4 photosynthesis in the spider plant (Figure 6F).
402
403 **DISCUSSION**
404 *G. gynandra* has been an instrumental organism for addressing evolutionary questions, often
405 as a pair with *T. hassleriana* (Hoang et al., 2022). This plant is valuable for the study of its
406 nutritional and health-promoting properties, as well as molecular mechanisms absent in C_3
407 model organisms such as the dicot *Arabidopsis* and the monocot rice, and represents an
408 emerging model plant to extensively investigate C_4 biology (Brown et al., 2005; Külahoglu et
409 al., 2014; Bayat et al., 2018). However, the lack of a high-quality chromosome-scale genome
410 of *G. gynandra* has hampered its wide adoption in basic and applied research. Here we report
411 a reference-grade genome of the diploid *G. gynandra* integrating long reads Nanopore
412 sequencing and Hi-C technologies to overcome the challenge inherent in highly repetitive
413 sequences (Figures 1 and 2). With a contig N50 of 11.43 Mb, scaffold N50 of 51.02 Mb and
414 LAI of 16.46, the assembly metrics indicate high accuracy and completeness (Table 1).
415 Genomics combined with transcriptomic analysis confirmed that *G. gynandra* is the typical
416 NAD-ME subtype of C_4 plant (Figure 6). Given that an *Agrobacterium tumefaciens*-mediated
417 transformation system with high efficiency has also been established for this elite crop
418 (Newell et al., 2010), *G. gynandra* is now suitable as a C_4 model system in dicotyledonous

419 plants, particularly for studies in NAD-ME subtype of C_4 species, such as the perennial
420 polyploid bioenergy crop switchgrass (*Panicum virgatum*).
421 The evolution of plant C_4 photosynthesis represents an unique example of convergent
422 evolution (Heyduk et al., 2019; Wang et al., 2009; Sage, 2004). With the availability of the
423 annotated genomes for *G. gynandra* and *T. hassleriana*, direct comparison between these C_4
424 and C_3 species presents an excellent model to unravel why C_4 photosynthesis evolved in only
425 one of the two plants. Instead of sharing a Th-α event (van den Bergh et al., 2014), these two
426 species experienced independent recent WGD (Gg-α) and WGT (Th-α) events, respectively
427 (Figure 3). However, massive gene loss may have happened in C_3 *T. hassleriana* after Th-α
428 (Supplemental Figure S18 and Supplemental Data Set S19), which resulted in retention of
429 only 27,396 predicted genes, making *T. hassleriana* the gene-poorest species of those
430 analyzed here (Figure 1D). Of note, the copy numbers of multiple C_4 pathway-related genes
431 are higher in *G. gynandra* relative to *T. hassleriana* (Supplemental Data Set S18), including
432 those involved in vasculature development (*PIN1*, *SCR* and *HB-8*), C_4 metabolism (*ALAAT*
433 and *NHD*), Calvin-Benson cycle (*RbcSSU*), N assimilation (*FdGOGAT*), S assimilation (*APR*
434 and *SR*), and photorespiration (*GDCP* and *SGAT*), concomitant with markedly reduced
435 expressions of these vasculature development and C_4 metabolism genes in *T. hassleriana*
436 (Supplemental Figure S20). Moreover, the Gg-α in *G. gynandra* contributed to the expansion
437 of some gene families shared with the C_4 monocot *Z. mays*, which function in various C_4
438 metabolism-associated processes from signaling pathways to photosynthetic performance and
439 stress resistance (Figure 4). This is supportive of recent studies showing that WGD led to
440 multiple aspects of the evolution of C_4 photosynthesis in *G. gynandra* and grasses (Huang et
441 al., 2021, 2022). Almost all of the well-documented vein development-associated genes in *G.*
442 *gynandra* have retained their WGD-derived duplicates (Supplemental Data Set S20) (Ohashi-
443 Ito and Fukuda, 2010; Huang et al., 2021; Liu et al., 2022). Importantly, some of these
444 paralogous genes that positively control vein density became significantly up-regulated in *G.*
445 *gynandra* compared to *T. hassleriana*, with those negative ones being dramatically down-
446 regulated (Supplemental Figure S12) (Huang et al., 2017; Aubry et al., 2014; Liu et al., 2020),
447 which may have conferred the much higher leaf vein density seen in *G. gynandra* (Figure 5,
448 B and C). Peculiarly, *G. gynandra* has retained the paralogous genes essential for building the
449 photorespiratory CO_2 pump in BS cells, such as *ALAAT*, *ASPAT*, *GOGAT* and *GDCP*
450 (Supplemental Data Sets S18 and S20) (Huang et al., 2021), whose formation is hypothesized
451 to be the primary driver of C_4 evolution (Mallmann et al., 2014; Sage et al., 2012). Although
452 the overall level of expression for photorespiration pathway genes in *G. gynandra* is down-

453 regulated, photorespiration is not and cannot be lost, as it has crucial functions in plants.
454 These data suggest that *G. gynandra* underwent the C_3-C_4 intermediate stage required to
455 establish the C_4 pathway. *G. gynandra* harbors three *GDCP* gene copies; however, only one
456 is highly expressed in BS cells, which exhibits gradually increased expression during leaf
457 development (Figure 6, C–E). It is speculated that the inactivated gene copy will eventually
458 be lost (Schulze et al., 2016; Mercado and Studer, 2022). Consistently, a single *GDCP* is
459 active in monocot C_4 species (maize, foxtail millet and sorghum) and in the dicot C_3-C_4
460 intermediate species *Flaveria* and *Moricandia* (Figure 6C) (Schulze et al., 2013; Schlüter et
461 al., 2017). These imply that the C_4 trait in *G. gynandra* could be still evolving. Additionally,
462 genomic analysis showed that the promoter regions of the *GDCP* genes in C_3, C_4 dicots and
463 C_4 monocots contained diverse *cis*-active element motifs (Figure 6C). While the V-box
464 element has been demonstrated to orchestrate the expression of *GDCP* in the vasculature of
465 *Moricandia* (Adwy et al., 2019, 2015), it is not found in *G. gynandra* or C_4 monocots,
466 implying that varied modes might have evolved to regulate cell-specific *GDCP* expression
467 not only between C_3 and C_4 species but also among C_4 plants.

468 Heat, intense light and/or drought stress were proposed to drive C_4 origination and
469 evolution during periods of declining atmospheric CO_2, suggesting the role of adaptive
470 evolution in C_4 pathway formation (Blätke and Bräutigam, 2019; Sage, 2004). Not surprising,
471 C_4 photosynthesis has better performance than the ancestral C_3 state under stressful
472 environments. This will be increasingly important under the projected conditions of long-
473 term climate change and periodic environmental extremes currently threatening the global
474 food supply and bioenergy security. *G. gynandra* displays much higher tolerance to extreme
475 temperature than *T. hassleriana*, and this phenotype is likely associated with retention of a
476 subset of WGD-duplicated genes in *G. gynandra* that encode HSFs and HSPs (Figure 5F and
477 Supplemental Data Set S20). Although their expressions can be induced under heat stress in
478 both species, many more of these families are up-regulated in *G. gynandra* compared to *T.*
479 *hassleriana* (Figure 5G). Given that C_4 photosynthesis in *G. gynandra* evolved after WGD
480 (van den Bergh et al., 2014), this provides additional evidence on the critical role of Gg-α in
481 facilitating C_4 evolution.

482 Aside from WGD event and the expanded gene families, recent species-specific tandem
483 duplications after Gg-α may also be relevant to maintenance of the C_4 pathway in *G.*
484 *gynandra*, exemplified by duplication of multiple key enzymes involved in carbon fixation
485 including NAD-MDH/mMDH1 and PEPC2 of C_4 cycle (Figure 3, E–G). Remarkably, our
486 data unveiled a previously undescribed role for genomic transposon expansion in the

487 evolution of C_4 photosynthesis. The higher frequency of LTR-RT insertion in promoter
488 regions of *G. gynandra* contributes to higher ratio of up-regulated than down-regulated genes
489 when compared to *T. hassleriana*, independent of leaf developmental stages. Of importance,
490 the up-regulated genes function in various pathways involved in C_4 photosynthesis, including
491 but not limited to, C_4 cycle, light reaction, cyclic electron flow, Calvin cycle, redox
492 regulation, auxin signaling, vein patterning and stress response, whereas LTR-RT-inserted
493 genes involved in photorespiration exhibit lower expressions (Figure 2). Besides, a small
494 portion of C_4 homologous genes that contain less and more LTR-RT insertions, whose
495 expressions are up-regulated and down-regulated, respetively (Supplemental Figure S6C).
496 Therefore, it is tempting to postulate that LTR-RT activity might have promoted the C_3-to-C_4
497 evolution via synergistic genomic and transcriptomic alterations. Consistent to the recent
498 reports demonstrating that modifications in *cis*-regulatory and non-coding regions are
499 primary determinants of the distinct transcriptome blueprint in BSC or MC of C_4 plants (Tu
500 et al., 2020; Dickinson et al., 2020; Dai et al., 2022), this extensive LTR-RT insertion
501 frequency in promoter regions appears to be a underappreciated route through which cell-
502 preferential gene expression could be achieved. Future molecular characterization of
503 regulatory regions containing LTR-RTs will be required to test this hypothesis. Altogether,
504 our present study suggests a three-step scenario contributing to the evolution of C_4
505 photosynthesis in the *Cleome* genus and that innovation of this novel biochemical pathway in
506 *G. gynandra* may be dual consequences of duplicated gene retention and functional changes
507 in existing genes (Figure 6F).

508 In summary, we have generated a highly continuous and accurate genome assembly of the
509 C_4 model crop *G. gynandra*. Systematic comparison with the closely related C_3 species *T.*
510 *hassleriana* is useful for identification of previously uncharacterized genes involved in C_4
511 photosynthesis-related processes. Moreover, we present evidence that LTR-RT bursts have
512 functioned in driving genome size increase and may have been important for C_4 evolution as
513 well. WGD, gene family expansion and tandem duplication events have also facilitated the
514 evolution of C_4 photosynthesis in *G. gynandra*. We found corresponding transcriptional
515 changes of gene expression features associated with C_4 pathway, photorespiration, vein
516 venation and heat stress response for boosting photosynthetic efficiency. These findings shed
517 light on the commonalities and differences in the evolution of C_4 photosynthesis, supporting
518 the existence of numerous independent evolutionary trajectories to C_4. The genomic and
519 transcriptomic data generated in this study provide valuable new resources for further
520 dissecting the genetic basis underlying the transition from C_3 to C_4 photosynthesis as well as

521 the exceptional nutritional and medicinal traits of this species. *G. gynandra* is thus now a
522 promising model species to accelerate both basic and applied research, in C_4 biology and
523 beyond.
524
525 **MATERIALS AND METHODS**
526 **Plant materials and growth conditions**
527 C_4 *Gynandropsis gynandra* Linn. and C_3 *Tarenaya hassleriana* (Purple Queen) species were
528 grown in plastic pots with Pro-Mix BX soil, in a controlled environment room with a
529 photoperiod of 16h/8h, a light intensity of 200 μmol m^{-2} s^{-1}, 25/18 °C (day/night), and a
530 humidity of 50–60%. The leaves (4 weeks), stems (4 weeks), roots (4 weeks), flower buds (6
531 weeks), flowers (7 weeks) and siliques (10 weeks) of plants were harvested and immediately
532 frozen in liquid nitrogen.
533 **Heat treatment**
534 5-week-old plants of both species were transferred to a growth chamber (PercivalE-41, USA)
535 using the conditions above, except with the day/night temperature set to 45/35 °C, which is
536 10–15 °C above optimum range of germination for *G. gynandra* and is considered as heat
537 stress (Motsa et al., 2015). Leaves at different developmental stages were sampled from
538 plants at 10:00 am before and after heat treatment. Meanwhile, leaf samples at the equivalent
539 stages under normal growth conditions were collected as controls (Supplemental Figure S11).
540 Stages 1 to 5 (S1 to S5) were leaves from young to mature, with Stage 1 as the youngest (1.5
541 cm in length). All experiments were performed in triplicate.
542 **RNA-Seq analysis**
543 For RNA-Seq experiments, total RNAs were extracted and purified from the collected leaf
544 samples above using Trizol RNA extraction kit (Invitrogen, Carlsbad, CA, USA). The mRNA
545 was enriched from approximately 50 ng of high-quality total RNA with NEXTflex™ Poly(A)
546 Beads (Bioo Scientific, Austin, TX, USA), and used to produce RNA-seq libraries with the
547 NEBNext Ultra RNA Library Prep Kit for Illumina (New England Biolabs, Ipswich, MA,
548 USA) according to the manufacturer's protocol. The RNA-Seq libraries were sequenced with
549 Illumina HiSeq4000 (Illumina, San Diego, CA, USA) under PE150 mode. The raw reads of
550 RNA-seq were filtered using Trimmomatic (version 0.40) with default parameters (Bolger et
551 al., 2014). The remaining clean reads were mapped to the genome using HISAT2 (version
552 2.1.0) (Kim et al., 2019). The reads count per gene was calculated with HTSeq (version
553 0.9.172) (Anders et al., 2015). The differentially expressed genes (DEGs) were identified

554 using the DEseq2 package with a significance threshold of q value < 0.01 and $|\log_2(\text{fold}$
555 $\text{change})| > 1$ (Love et al., 2014).

556 **Iso-Seq analysis**

557 Total RNAs extracted from different tissues collected above were combined to generate a full
558 RNA sample of *G. gynandra*. The mRNA was enriched from total RNA using a magnetic d(T)
559 bead binding procedure, and then was transcribed to cDNA using the Clontech SMARTer
560 PCR cDNA Synthesis Kit (Clontech, Mountain View, CA, USA) following the
561 manufacturer's instructions. The amplified cDNA fragments were size-selected using a
562 BluePippin Size Selection System (Sage Science, Massachusetts, United States) with a bin
563 of >4 kb. The amplified and size-selected cDNA products were used to generate SMRT Bell
564 libraries according to the Iso-Seq protocol (P/N100-377-100-05 and P/N100-377-100-04).
565 The libraries were prepared for sequencing by annealing a sequencing primer and binding
566 polymerase to the SMRT bell templates using the DNA/Polymerase Binding Kit (Pacific
567 Biosciences, Menlo Park, CA, USA). One SMRT cell was sequenced on the PacBio Sequel
568 instrument (Pacific Biosciences, Menlo Park, CA, USA). The high-quality, full-length and
569 consistent transcript sequences were obtained from long reads data using the PacBio Iso-Seq3
570 pipeline.

571 **Genome sequencing**

572 Nanopore, Illumina HiSeq and Hi-C were used for sequencing the complete genome of *G.*
573 *gynandra*. For Illumina sequencing library construction, the genomic DNA of *G. gynandra*
574 was extracted from young leaves using a Qiagen DNA purification kit (Qiagen, Darmstadt,
575 Germany). The integrity of DNA was assessed by agarose gel electrophoresis, and the purity
576 and concentration were determined on NanoDrop 2000 spectrophotometer (Thermo Fisher
577 Scientific, MA, USA) and Qubit Fluorometer (Invitrogen, Carlsbad, CA, USA), respectively.
578 The short-read genomic sequencing libraries were constructed using the MGIEasy FS DNA
579 Library Prep Set (Item No.1000006988) with 270 bp fragment size according to the
580 manufacturer's instructions, and sequenced on an Illumina Hiseq4000 platform (Illumina,
581 San Diego, CA) to generate paired-end (PE) reads of 150 bp. For Nanopore sequencing
582 library preparation, the high-quality genomic DNA of *G. gynandra* was extracted from young
583 leaves using the CTAB method. Approximately 15 μg of genomic DNA was used to collect
584 larger DNA fragments (>20 kb) with the BluePippin Size-Selection system (Sage science,
585 Beverly, MA, USA). The obtained genomic DNA was processed using ONT Ligation
586 Sequencing Kit (SQK-LSK109; Oxford Nanopore Technologies, Oxford, United Kingdom)
587 according to the manufacturer's instructions. Briefly, the genomic DNA was end-repaired

588 and dA-tailed using a NEBNext UltraII End Prep Reaction Module (New England Biolabs,
589 Ipswich, MA, USA). The sequencing adaptors were ligated using NEBNext UltraII Ligation
590 module (New England Biolabs, Ipswich, MA, USA). Libraries were purified using AMpure
591 XP beads (Beckman Coulter , California, USA) and short fragment buffer (SFB). Then,
592 Nanopore libraries were added into a single ONT MinION R9.4 flowcell (FLO-MIN106) and
593 sequenced on the platform of PromethION (Oxford Nanopore Technologies, UK). The ONT
594 MinKNOW software (https://github.com/nanoporetech/minknow_lims_interface.git)
595 acquired raw sequence data with live basecalling by ONT Guppy (https://nanoporetech.com/).
596 For Hi-C sequencing, the fresh leaf tissues of *G. gynandra* were fixed (cross-linking) with
597 formaldehyde. The cross-linked chromatin was extracted and digested by *Mbo*I restriction
598 enzyme, the 5' overhangs filled in with biotinylated nucleotides, and blunt-end proximity-
599 ligated to generate circular molecules. Subsequently, the circular DNA molecules were
600 purified from protein, and sheared to ~350 bp mean fragment size, and then enriched by
601 biotin pull down. The sequencing libraries were generated using NEBNext Ultra enzymes
602 (New England Biolabs, Ipswich, MA, USA) and Illumina-compatible adapters (Illumina, San
603 Diego, CA, USA). The Hi-C libraries were processed to paired-end sequencing on the
604 Illumina Hiseq 4000 (Illumina, San Diego, CA, USA) platform with read length of 150 bp.

605 **Genome size estimation**

606 The genome size of *G. gynandra* was estimated using the *k*-mer analysis. Raw reads from
607 Illumina sequencing were subjected to SOAPnuke (https://github.com/BGI-
608 flexlab/SOAPnuke) for base quality control. The genome size, abundance of repetitive
609 elements and heterozygosity were estimated based on the *k*-mer frequencies generated from
610 the short reads using GenomeScope (https://github.com/schatzlab/genomescope).

611 ***De novo* genome assembly**

612 The ONT long reads were corrected and assembled using CANU (version 1.7.1) with the
613 parameters (corOutCoverage=50, saveOverlaps=TRUE, ovsMemory=64, minMemory=30G,
614 batMemory=200G, minOverlapLength=700, minReadLength=1000) (Koren et al., 2017).
615 The resulting contigs were polished with both long reads and short reads using three rounds
616 of Racon (version 1.4.13) with default parameters (Vaser et al., 2017). The Illumina short
617 reads were mapped onto the polished assembly with BWA-MEM (https://github.com/bwa-
618 mem2/bwa-mem2). Based on the alignment, error correction was conducted using Pilon
619 (version 1.23) (Walker et al., 2014). To scaffold the assembled contigs, the ONT-based
620 polished contigs were anchored into a chromosome-scale assembly using a Hi-C proximity-
621 based assembly approach. Illumina reads from the Hi-C library were processed with

622 SOAPnuke to remove adaptor and low-quality sequences. The clean Hi-C read pairs were
623 used as input for the Juicer (version 1.6) and 3d-DNA Hi-C analysis and scaffolding pipelines
624 (version 180922) (Dudchenko et al., 2017; Durand et al., 2016). Valid interaction pairs were
625 mapped onto the polished contigs and anchored to the pseudo-chromosomes using 3d-DNA
626 pipeline with default parameters. The Hi-C interaction matrix was visualized using Juicebox
627 Assembly Tools, and mis-assemblies and mis-joins were manually corrected based on
628 neighboring interactions to generate the final pseudo-chromosome-length genome assembly.

629 **Genome assembly quality assessment**

630 Three assessment strategies including BUSCO alignment, transcriptome alignment and LTR
631 assembly index, were used to evaluate the quality and completeness of the *G. gynandra*
632 genome assembly. In brief, the completeness of the genome assembly was evaluated using
633 the BUSCO pipeline based on the datasets of embryophyta_odb10. The coverage and base-
634 level accuracy of the genome assembly were assessed by aligning transcriptome reads to the
635 *G. gynandra* assembly using HISAT2 with default parameters. LAI score of the *G. gynandra*
636 genome assembly was calculated using LTR_retriever (version 2.9.0) with default parameters
637 (Ou and Jiang, 2018).

638 **Genome annotation**

639 The *G. gynandra* genome was annotated including annotations of repeat sequences, protein-
640 coding genes and RNA genes. First, we adopted two complementary methods (one
641 homology-based and the other *de novo*-based) to predict repeat sequences. RepeatMasker
642 (version 4.0.7) and RepeatProteinMask (http://www.repeatmasker.org) were used to discover
643 and classify repetitive sequences with the homology-based library generated from Repbase
644 (www.girinst.org/repbase) (Bedell et al., 2000). LTR_FINDER (version 1.06) and
645 RepeatModeler (http://www.repeatmasker.org/RepeatModeler) were utilized to build the *de*
646 *novo*-based library (Xu and Wang, 2007). TRF (version 4.09) was employed to annotate
647 tandem repeats with default parameters (Benson, 1999). Full length LTR-RTs were identified
648 using LTR_retriever. Second, we deployed a strategy combining *ab initio*, homology-based
649 and transcriptome-based methods for gene structure annotation. We used both Augustus
650 (version 3.3.2) and SNAP (version 1.0.4) to perform *ab initio* predictions with self-trained
651 prediction models (Stanke et al., 2004; Korf, 2004). We aligned the protein sequences from *A.*
652 *thaliana*, *B. oleracea*, *B. rapa*, *T. hassleriana*, *G. raimondii*, *M. Sativa*, *S. lycopersicum*, *O.*
653 *sativa* and *Z. mays* to the repeat-masked genome of *G. gynandra*, and then parsed the
654 resultant alignments by GeneWise (https://www.ebi.ac.uk/~birney/wise2/) to achieve
655 homolog predictions. We mapped the transcripts generated from both PacBio Iso-Seq and

656 Illumina RNA-Seq to the genome with PASA (version r20140407) to conduct transcriptome-
657 based predictions (Haas et al., 2008). Finally, we combined all the evidences to finalize the
658 consensus gene models using Maker (version 2.31.9) (Cantarel et al., 2008). Third, we
659 performed RNA genes annotation by tRNAscan-SE (version 2.0) for tRNA (Lowe and Chan,
660 2016), RNAmmer (version 1.2) for rRNA (Lagesen et al., 2007), and INFERNAL (version
661 1.1.2) for miRNA and snRNA (Nawrocki and Eddy, 2013). In addition, we annotated
662 transcription factor encoding genes using iTAK (version 1.7) (Zheng et al., 2016). We
663 generated functional assignments of protein coding genes by performing BLAST searches
664 against five public protein databases including the NCBI non-redundant (nr) database,
665 SwissProt database, Clusters of Orthologous Genes (COG) database, KEGG database and
666 GO database. Pfam domains of genes were identified using InterProScan.

667 **Phylogenomic evolution analysis**

668 Orthology prediction for ten species including eight eudicots (*A. thaliana*, *B. oleracea*, *B.*
669 *rapa*, *G. gynandra*, *T. hassleriana*, *G. raimondii*, *M. Sativa* and *S. lycopersicum*), two
670 monocots (*O. sativa* and *Z. mays*) was performed using OrthoFinder (version 2.2.6) package
671 with default parameters (Emms and Kelly, 2019). Single-copy orthologous genes were
672 extracted from the clustering results, and were used to reconstruct the phylogenetic tree. In
673 brief, the proteins of single-copy gene families were aligned by MUSCLE (version 3.8.31)
674 (Edgar, 2004). The alignments were finally joined into a super gene matrix for the species
675 phylogenetic tree construction using RAxML (version 8.2.12) (Stamatakis, 2014) with the
676 JTT+I+GAMMA model and 1,000 bootstrap replicates. The best suitable evolution model for
677 phylogeny construction was evaluated using jModelTest (version 2.1.10) (Darriba et al.,
678 2012). Time estimation among species was performed with r8s (version 1.81) (Sanderson,
679 2003). The divergence times of *B. oleracea* and *B. rapa* (2.02–3.21 MYA), *Z. mays* and *O.*
680 *sativa* (42–52 MYA) and *A. thaliana* and *O. sativa* (115–308 MYA) obtained from TimeTree
681 (http://timetree.org) were used for calibration. Syntenic blocks and gene duplications were
682 identified within the *G. gynandra* genome or between the *Cleome* plants and other species
683 using MCScanX (version 0.8) with the parameters (-s 5, -m 5) (Wang et al., 2012). The
684 synonymous mutation rate values for gene pairs within syntenic blocks were calculated using
685 the PAML (version 4.9) with yn00 and NG model (Yang, 2007). Fourfold degenerative
686 transversion (4DTv) rates were calculated by aligning all orthologous or paralogous gene
687 pairs using an in-house Perl script. We identified the WGD event within the *G. gynandra*
688 genome using the approach from PGDD (Lee et al., 2013). CAFE (version 4.2.1) was used to
689 identify the gene families with rapid expansion or contraction based on the species

690 phylogenetic tree and divergence time (De Bie et al., 2006). The species-specific gene
691 families were determined according to the presence and absence of genes for specific species.

692 **Analysis of leaf anatomy**

693 Leaf samples were rinsed twice in water and placed in 70% ethyl alcohol for 3–4 days. The
694 70% ethyl alcohol was changed every eight hours until the leaves became colorless and
695 transparent. Leaves were rinsed again with water and mounted in 66% glycerol on slides for
696 observation. Images of the cleared leaves were taken with an OLYMPUS BX43 microscope
697 system equipped with an OLYMPUS DP74 camera at 2× magnification (Olympus, Tokyo,
698 Japan). Vein length and area size were assessed for six sites at a central region of each leaf
699 bounded by the midvein using phenoVein tools developed from MeVisLab
700 (www.mevislab.de) (Bühler et al., 2015). Vein density (Vd) was calculated as the total length
701 of all veins within the region divided by the area of the region, which was expressed in mm
702 mm^{-2}. Measurements were conducted with three independent leaves of each stage per species.

703 **Phylogenetic and cis-acting regulatory elements analysis**

704 The protein sequences of *GDCP* genes were used to perform multiple sequence alignment
705 using MUSCLE. Phylogenetic tree was inferred using the Neighbor-Joining (NJ) method
706 available in MEGA7 (version 7.0.26) (Kumar et al., 2016). The robustness of each node in
707 the tree was determined using 1000 bootstrap replicates. The upstream 1.5 kb regions from
708 transcription start site (TSS) of each *GDCP* gene were extracted from genome sequence of
709 each species, and used to identify conserved motifs using MEME, and *cis*-acting regulatory
710 elements by PlantCARE server (http://bioinformatics.psb.ugent.be/webtools/plantcare/html).

711

712 **Accession Numbers**

713 All sequence information has been uploaded to Genome Sequence Archive
714 (https://bigd.big.ac.cn/gsa). Genomic data: *Gynandropsis gynandra*-PRJCA008306;
715 Transcriptomic data: *Gynandropsis gynandra*-PRJCA008307; *Tarenaya hassleriana*-
716 PRJCA008308. The chromosome-scale annotated genome assembly of *Gynandropsis*
717 *gynandra* is available at the Genome Warehouse in the National Genomics Data Center
718 (https://ngdc.cncb.ac.cn) under accession number GWHBHRJ00000000.

719

720 **Supplemental Files**

721 Supplemental Figure S1. Statistics for the frequencies and depths of 15 *k*-mers in the *G.*
722 *gynandra* genome.

723 Supplemental Figure S2. Overview of the processing pipeline for assembling the *G. gynandra*
724 genome.
725 Supplemental Figure S3. Length distribution of ONT sequencing reads.
726 Supplemental Figure S4. KEGG functional enrichment analysis of gene families specific to *G.*
727 *gynandra*.
728 Supplemental Figure S5. The density distribution of intact LTRs, *Gypsy* and *Copia* in each
729 chromosome of *G. gynandra*.
730 Supplemental Figure S6. Genomic distribution of LTR-RTs and their impacts on expression
731 patterns of the C_4 pathway-associated genes in *G. gynandra* compared to *T. hassleriana*.
732 Supplemental Figure S7. Comparative genomic analysis of the WGD event in *G. gynandra*.
733 Supplemental Figure S8. Functional enrichment of WGD-derived genes and expression
734 analysis of TD-derived genes in *G. gynandra*.
735 Supplemental Figure S9. MapMan-Bin enrichment analysis of 221 expanded gene families
736 common to *G. gynandra* and *Z. mays*.
737 Supplemental Figure S10. Representative anatomy of the leaf cross-section of *G. gynandra*
738 and *T. hassleriana*.
739 Supplemental Figure S11. The morphology of leaves at different developmental stages for *G.*
740 *gynandra* and *T. hassleriana*.
741 Supplemental Figure S12. The expression patterns of leaf and vasculature-related regulatory
742 genes along leaf development gradients for *G. gynandra* and *T. hassleriana*.
743 Supplemental Figure S13. The gene regulatory networks (GRNs) between transcription
744 factors and their candidate target genes in *G. gynandra* or *T. hassleriana*.
745 Supplemental Figure S14. Enrichment of *Vdof1* gene in leaf BS cells.
746 Supplemental Figure S15. Overexpression of *Vdof1* gene led to enhanced photosynthetic
747 capacity, leaf vein density and tolerance to heat stress.
748 Supplemental Figure S16. MapMan-Bin enrichment analysis of DEGs at different stages of
749 leaves from *G. gynandra* and *T. hassleriana* subjected to heat stress.
750 Supplemental Figure S17. Heatmap showing expression patterns of C_4 photosynthesis-related
751 pathway genes under heat stress in *G. gynandra* and *T. hassleriana*.
752 Supplemental Figure S18. Copy number ratio of genes for C_4 photosynthesis-related
753 pathways in *G. gynandra* as compared to *T. hassleriana*.
754 Supplemental Figure S19. Phylogenetic trees of C_4 photosynthesis-related genes.
755 Supplemental Figure S20. The expression levels of C_4 pathway-related genes with lower
756 copy numbers in *T. hassleriana* than in *G. gynandra* along leaf development gradients.

757 Supplemental Data Set S1. Estimate of *G. gynandra* genome size.
758 Supplemental Data Set S2. The evaluation of ONT sequencing data for *G. gynandra*.
759 Supplemental Data Set S3. Statistics of Hi-C data for *G. gynandra*.
760 Supplemental Data Set S4. Summary of *G. gynandra* genome assembly.
761 Supplemental Data Set S5. Summary of *G. gynandra* seventeen pseudo-chromosomes.
762 Supplemental Data Set S6. BUSCO analysis of *G. gynandra* genome assembly.
763 Supplemental Data Set S7. RNA-seq data mapping summary.
764 Supplemental Data Set S8. Functional annotation of the predicted genes in the assembly of *G.*
765 *gynandra* genome.
766 Supplemental Data Set S9. Statistics of the annotated non-coding RNAs.
767 Supplemental Data Set S10. Gene numbers of transcription factor family among *G. gynandra*
768 and nine other species.
769 Supplemental Data Set S11. Numbers of gene families among *G. gynandra* and nine other
770 species.
771 Supplemental Data Set S12. Summary of repeat DNA in *G. gynandra* and *T. hassleriana*.
772 Supplemental Data Set S13. List of gene IDs and their RPKM values in leaf transcriptomes
773 from S0 to S5 developmental stages of *G. gynandra* and *T. hassleriana*.
774 Supplemental Data Set S14. Syntenic blocks of *G. gynandra*.
775 Supplemental Data Set S15. Pfam annotation of the expanded genes families in *G. gynandra*
776 genome.
777 Supplemental Data Set S16. The hub genes of *Dof*-GRNs of *G. gynandra* and *T. hassleriana*.
778 Supplemental Data Set S17. Summary of differentially expressed genes after heat stress
779 treatment at different leaf stages in *G. gynandra* and *T. hassleriana*.
780 Supplemental Data Set S18. Copy numbers of genes that regulate vasculature development,
781 C_4 photosynthesis and heat shock response in *G. gynandra* compared to *T. hassleriana*.
782 Supplemental Data Set S19. Statistics analysis suggesting that *T. hassleriana* may have
783 undergone massive gene loss compared to *G. gynandra*.
784 Supplemental Data Set S20. Genes that regulate vasculature development, C_4 photosynthesis
785 and heat shock response were mostly derived from WGD in *G. gynandra*.
786 Supplemental Data Set S21. Abbreviations of genes and protein enzymes in this study.
787

788 **ACKNOWLEDGEMENTS**

789 We thank Prof. Y. Jiao at Henan Agricultural University and Prof. S. Gao at Henan
790 University of Science and Technology for providing G. gynandra and T. hassleriana seeds

used in this study. The bioinformatic analyses are performed with the supercomputing system in the Supercomputing Center of Oil Crops Research Institute, Chinese Academy of Agricultural Sciences.

FUNDING

This work was supported by the Agricultural Science and Technology Innovation Project of the Chinese Academy of Agricultural Sciences (Grant CAAS-ASTIP-OCRI) and the National Natural Science Foundation of China (Grant 32072096).

AUTHOR CONTRIBUTIONS

W.H., J.Liu, and W.Z. conceived project. W.H., J.Liu, and W.Z. designed study. J.Li, X.S. and Q.Z. conducted experiments. W.Z. and J.Liu performed data analysis. W.Z. and J.Liu wrote and revised the manuscript.

DECLARATION OF INTERESTS

The authors declare no competing interests.

REFERENCES

Adwy, W., Laxa, M., and Peterhansel, C. (2015). A simple mechanism for the establishment of C_2-specific gene expression in Brassicaceae. *Plant J*. **84**: 1231–1238.

Adwy, W., Schlüter, U., Papenbrock, J., Peterhansel, C., and Offermann, S. (2019). Loss of the M-box from the glycine decarboxylase P-subunit promoter in C_2 *Moricandia* species. *Plant Gene* **18**: 100176.

Anders, S., Pyl, P.T., and Huber, W. (2015). HTSeq-A Python framework to work with high-throughput sequencing data. *Bioinformatics* **31**: 166–169.

Aubry, S., Kelly, S., Kümpers, B.M.C., Smith-Unna, R.D., and Hibberd, J.M. (2014). Deep Evolutionary Comparison of Gene Expression Identifies Parallel Recruitment of Trans-Factors in Two Independent Origins of C_4 Photosynthesis. *PLoS Genet*. **10**: e1004365.

Bayat, S., Schranz, M.E., Roalson, E.H., and Hall, J.C. (2018). Lessons from Cleomaceae, the Sister of Crucifers. *Trends Plant Sci*. **23**: 808–821.

Bedell, J.A., Korf, I., and Gish, W. (2000). MaskerAid: A performance enhancement to RepeatMasker. *Bioinformatics* **16**: 1040–1041.

Bennetzen, J.L. et al. (2012). Reference genome sequence of the model plant Setaria. *Nat. Biotechnol*. **30**:555–561.

Benson, G. (1999). Tandem repeats finder: A program to analyze DNA sequences. *Nucleic Acids Res*. **27**: 573–580.

826 **van den Bergh, E., Külahoglu, C., Bräutigam, A., Hibberd, J.M., Weber, A.P.M., Zhu, X.G., and Schranz,**
827 **M.E.** (2014). Gene and genome duplications and the origin of C_4 photosynthesis: Birth of a trait in the
828 Cleomaceae. *Curr. Plant Biol*. **1**: 2–9.
829 **De Bie, T., Cristianini, N., Demuth, J.P., and Hahn, M.W.** (2006). CAFE: A computational tool for the study
830 of gene family evolution. *Bioinformatics* **22**: 1269–1271.
831 **Blätke, M.A. and Bräutigam, A.** (2019). Evolution of C_4 photosynthesis predicted by constraint-based
832 modelling. *Elife* **8**: e49305.
833 **Bolger, A.M., Lohse, M., and Usadel, B.** (2014). Trimmomatic: A flexible trimmer for Illumina sequence data.
834 *Bioinformatics* **30**: 2114–2120.
835 **Bräutigam, A. et al.** (2011). An mRNA blueprint for C_4 photosynthesis derived from comparative
836 transcriptomics of closely related C_3 and C_4 species. *Plant Physiol*. **155**: 142–156.
837 **Brown, N.J., Parsley, K., and Hibberd, J.M.** (2005). The future of C_4 research - Maize, *Flaveria* or *Cleome*?
838 *Trends Plant Sci*. **10**: 215–221.
839 **Bühler, J., Rishmawi, L., Pflugfelder, D., Huber, G., Scharr, H., Hülskamp, M., Koornneef, M., Schurr,**
840 **U., and Jahnke, S.** (2015). Phenovein—a tool for leaf vein segmentation and analysis. *Plant Physiol*. **169**:
841 2359–2370.
842 **Cantarel, B.L., Korf, I., Robb, S.M.C., Parra, G., Ross, E., Moore, B., Holt, C., Alvarado, A.S., and**
843 **Yandell, M.** (2008). MAKER: An easy-to-use annotation pipeline designed for emerging model organism
844 genomes. *Genome Res*. **18**: 188–196.
845 **Cheng, S. et al.** (2013). The *Tarenaya hassleriana* genome provides insight into reproductive trait and genome
846 evolution of crucifers. *Plant Cell* **25**: 2813–2830.
847 **Dai, X., Tu, X., Du, B., Dong, P., Sun, S., Wang, X., Sun, J., Li, G., Lu, T., Zhong, S., and Li, P.** (2022).
848 Chromatin and regulatory differentiation between bundle sheath and mesophyll cells in maize. *Plant J*.
849 **109**: 675–692.
850 **Darriba, D., Taboada, G.L., Doallo, R., and Posada, D.** (2012). JModelTest 2: More models, new heuristics
851 and parallel computing. *Nat. Methods* **9**: 772.
852 **Dickinson, P.J., Kneřová, J., Szecówka, M., Stevenson, S.R., Burgess, S.J., Mulvey, H., Bågman, A.M.,**
853 **Gaudinier, A., Brady, S.M., and Hibberd, J.M.** (2020). A bipartite transcription factor module
854 controlling expression in the bundle sheath of *Arabidopsis thaliana*. *Nat. Plants* **6**: 1468–1479.
855 **Dudchenko, O., Batra, S.S., Omer, A.D., Nyquist, S.K., Hoeger, M., Durand, N.C., Shamim, M.S., Machol,**
856 **I., Lander, E.S., Aiden, A.P., and Aiden, E.L.** (2017). *De novo* assembly of the *Aedes aegypti* genome
857 using Hi-C yields chromosome-length scaffolds. *Science* **356**: 92–95.
858 **Durand, N.C., Shamim, M.S., Machol, I., Rao, S.S.P., Huntley, M.H., Lander, E.S., and Aiden, E.L.** (2016).
859 Juicer Provides a One-Click System for Analyzing Loop-Resolution Hi-C Experiments. *Cell Syst*. **3**: 95–
860 98.
861 **Edgar, R.C.** (2004). MUSCLE: Multiple sequence alignment with high accuracy and high throughput. *Nucleic*
862 *Acids Res*. **32**: 1792–1797.
863 **Emms, D.M. and Kelly, S.** (2019). OrthoFinder: Phylogenetic orthology inference for comparative genomics.
864 *Genome Biol*. **20**: 238.

865 **Ermakova, M., Danila, F.R., Furbank, R.T., and von Caemmerer, S.** (2020). On the road to C_4 rice:
866 advances and perspectives. *Plant J.* **101**: 940–950.
867 **Furbank, R.T.** (2011). Evolution of the C_4 photosynthetic mechanism: are there really three C_4 acid
868 decarboxylation types? *J. Exp. Bot*. **62**: 3103–3108.
869 **Haas, B.J., Salzberg, S.L., Zhu, W., Pertea, M., Allen, J.E., Orvis, J., White, O., Robin, C.R., and**
870 **Wortman, J.R.** (2008). Automated eukaryotic gene structure annotation using EVidenceModeler and the
871 Program to Assemble Spliced Alignments. *Genome Biol*. **9**: R7.
872 **Heyduk, K., Moreno-Villena, J.J., Gilman, I.S., Christin, P.A., and Edwards, E.J.** (2019). The genetics of
873 convergent evolution: insights from plant photosynthesis. *Nat. Rev. Genet*. **20**: 485–493.
874 **Hibberd, J.M., Sheehy, J.E., and Langdale, J.A.** (2008). Using C_4 photosynthesis to increase the yield of rice-
875 rationale and feasibility. *Curr. Opin. Plant Biol*. **11**: 228–231.
876 **Hoang, N. V et al.** (2022). The genome of *Gynandropsis gynandra* provides insights into whole-genome
877 duplications and the evolution of C_4 photosynthesis in Cleomaceae. *bioRxiv*: 2022.07.09.499295.
878 **Huang, C.F., Liu, W.Y., Lu, M.Y.J., Chen, Y.H., Ku, M.S.B., and Li, W.H.** (2021). Whole-Genome
879 Duplication Facilitated the Evolution of C_4 Photosynthesis in *Gynandropsis gynandra*. *Mol. Biol. Evol*. **38**:
880 4715–4731.
881 **Huang, C.F., Yu, C.P., Wu, Y.H., Lu, M.Y.J., Tu, S.L., Wu, S.H., Shiu, S.H., Ku, M.S.B., and Li, W.H.**
882 (2017). Elevated auxin biosynthesis and transport underlie high vein density in C_4 leaves. *Proc. Natl. Acad.*
883 *Sci. U. S. A*. **114**: E6884–E6891.
884 **Huang, W. et al.** (2022). A well-supported nuclear phylogeny of Poaceae and implications for the evolution of
885 C_4 photosynthesis. *Mol. Plant* **15**: 755–777.
886 **Hüdig, M., Tronconi, M.A., Zubimendi, J.P., Sage, T.L., Poschmann, G., Bickel, D., Gohlke, H., and**
887 **Maurino, V.G.** (2022). Respiratory and C_4-photosynthetic NAD-malic enzyme coexist in bundle sheath
888 cell mitochondria and evolved via association of differentially adapted subunits. *Plant Cell* **34**: 597–615.
889 **Jaillon, O. et al.** (2007). The grapevine genome sequence suggests ancestral hexaploidization in major
890 angiosperm phyla. *Nature* **449**: 463–467.
891 **Jiao, Y. et al.** (2011). Ancestral polyploidy in seed plants and angiosperms. *Nature* **473**: 97–100.
892 **Jiao, Y. et al.** (2017). Improved maize reference genome with single-molecule technologies. *Nature* **546**: 524–
893 527.
894 **Kim, D., Paggi, J.M., Park, C., Bennett, C., and Salzberg, S.L.** (2019). Graph-based genome alignment and
895 genotyping with HISAT2 and HISAT-genotype. *Nat. Biotechnol*. **37**: 907–915.
896 **Koren, S., Walenz, B.P., Berlin, K., Miller, J.R., Bergman, N.H., and Phillippy, A.M.** (2017). Canu:
897 Scalable and accurate long-read assembly via adaptive *k*-mer weighting and repeat separation. *Genome*
898 *Res*. **27**: 722–736.
899 **Korf, I.** (2004). Gene finding in novel genomes. *BMC Bioinformatics* **5**: 59.
900 **Koteyeva, N.K., Voznesenskaya, E. V., Roalson, E.H., and Edwards, G.E.** (2011). Diversity in forms of C_4
901 in the genus *Cleome* (Cleomaceae). *Ann. Bot*. **107**: 269–283.
902 **Külahoglu, C. et al.** (2014). Comparative transcriptome atlases reveal altered gene expression modules between
903 two Cleomaceae C_3 and C_4 plant species. *Plant Cell* **26**: 3243–3260.

904 **Kumar, S., Stecher, G., and Tamura, K.** (2016). MEGA7: Molecular Evolutionary Genetics Analysis Version
905 7.0 for Bigger Datasets. *Mol. Biol. Evol*. **33**: 1870–1874.
906 **Lagesen, K., Hallin, P., Rødland, E.A., Stærfeldt, H.H., Rognes, T., and Ussery, D.W.** (2007). RNAmmer:
907 Consistent and rapid annotation of ribosomal RNA genes. *Nucleic Acids Res*. **35**: 3100–3108.
908 **Lee, T.H., Tang, H., Wang, X., and Paterson, A.H.** (2013). PGDD: A database of gene and genome
909 duplication in plants. *Nucleic Acids Res*. **41**: D1152–D1158.
910 **Liu, W.-Y., Lin, H.-H., Yu, C.-P., Chang, C.-K., Chen, H.-J., Lin, J.-J., Lu, M.-Y.J., Tu, S.-L., Shiu, S.-H.,**
911 **Wu, S.-H., Ku, M.S.B., and Li, W.-H.** (2020). Maize ANT1 modulates vascular development,
912 chloroplast development, photosynthesis, and plant growth. Proc. Natl. Acad. Sci. **117**: 21747–21756.
913 **Liu, W.-Y., Yu, C.-P., Chang, C.-K., Chen, H.-J., Li, M.-Y., Chen, Y.-H., Shiu, S.-H., Ku, M.S.B., Tu, S.-**
914 **L., Lu, M.-Y.J., and Li, W.-H.** (2022). Regulators of early maize leaf development inferred from
915 transcriptomes of laser capture microdissection (LCM)-isolated embryonic leaf cells. *Proc. Natl. Acad.*
916 *Sci. U. S. A*. **119**: e2208795119.
917 **Love, M.I., Huber, W., and Anders, S.** (2014). Moderated estimation of fold change and dispersion for RNA-
918 seq data with DESeq2. *Genome Biol*. **15**: 550.
919 **Lowe, T.M. and Chan, P.P.** (2016). tRNAscan-SE On-line: integrating search and context for analysis of
920 transfer RNA genes. *Nucleic Acids Res*. **44**: W54–W57.
921 **Mallmann, J., Heckmann, D., Bräutigam, A., Lercher, M.J., Weber, A.P.M., Westhoff, P., and Gowik, U.**
922 (2014). The role of photorespiration during the evolution of C_4 photosynthesis in the genus *Flaveria*. *Elife*
923 **3**: e02478.
924 **Mamidi, S. et al.** (2020). A genome resource for green millet *Setaria viridis* enables discovery of agronomically
925 valuable loci. *Nat. Biotechnol*. **38**: 1203–1210.
926 **Marshall, D.M., Muhaidat, R., Brown, N.J., Liu, Z., Stanley, S., Griffiths, H., Sage, R.F., and Hibberd,**
927 **J.M.** (2007). *Cleome*, a genus closely related to *Arabidopsis*, contains species spanning a developmental
928 progression from C_3 to C_4 photosynthesis. *Plant J*. **51**: 886–896.
929 **Mercado, M.A. and Studer, A.J.** (2022). Meeting in the Middle: Lessons and Opportunities from Studying C_3-
930 C_4 Intermediates. *Annu. Rev. Plant Biol*. **73**: 43–65.
931 **Motsa, M.M., Slabbert, M.M., van Averbeke, W., and Morey, L.** (2015). Effect of light and temperature on
932 seed germination of selected African leafy vegetables. *South African J. Bot*. **99**: 29–35.
933 **Moyo, M. and Aremu, A.O.** (2021). Nutritional, phytochemical and diverse health-promoting qualities of
934 *Cleome gynandra*. *Crit. Rev. Food Sci. Nutr*. **62**: 3535–3552.
935 **Nawrocki, E.P. and Eddy, S.R.** (2013). Infernal 1.1: 100-fold faster RNA homology searches. *Bioinformatics*
936 **29**: 2933–2935.
937 **Newell, C.A., Brown, N.J., Liu, Z., Pflug, A., Gowik, U., Westhoff, P., and Hibberd, J.M.** (2010).
938 *Agrobacterium tumefaciens*-mediated transformation of *Cleome gynandra* L., a C_4 dicotyledon that is
939 closely related to *Arabidopsis thaliana*. *J. Exp. Bot*. **61**: 1311–1319.
940 **Ohashi-Ito, K. and Fukuda, H.** (2010). Transcriptional regulation of vascular cell fates. *Curr. Opin. Plant Biol*.
941 **13**: 670–676.
942 **Oshingi, S., Fekadu, F.D., Emmanuel, O.O., Traud, W., and Mary, O.A.-O.** (2019). *Cleome gynandra* L.
943 origin, taxonomy and morphology: A review. *African J. Agric. Res*. **14**: 1568–1583.

944 **Ou, S., Chen, J., and Jiang, N.** (2018). Assessing genome assembly quality using the LTR Assembly Index
945 (LAI). *Nucleic Acids Res*. **46**: e126.
946 **Ou, S. and Jiang, N.** (2018). LTR_retriever: A highly accurate and sensitive program for identification of long
947 terminal repeat retrotransposons. *Plant Physiol*. **176**: 1410–1422.
948 **Patchell, M.J., Roalson, E.H., and Hall, J.C.** (2014). Resolved phylogeny of Cleomaceae based on all three
949 genomes. Taxon **63**: 315–328
950 **Paterson, A.H. et al.** (2009). The *Sorghum bicolor* genome and the diversification of grasses. Nature **457**: 551–
951 556.
952 **Sage, R.F.** (2004). The evolution of C_4 photosynthesis. *New Phytol*. **161**: 341–370.
953 **Sage, R.F., Sage, T.L., and Kocacinar, F.** (2012). Photorespiration and the evolution of C_4 photosynthesis.
954 *Annu. Rev. Plant Biol*. **63**: 19–47.
955 **Sanderson, M.J.** (2003). r8s: Inferring absolute rates of molecular evolution and divergence times in the
956 absence of a molecular clock. *Bioinformatics* **19**: 301–302.
957 **Schlüter, U., Bräutigam, A., Gowik, U., Melzer, M., Christin, P.A., Kurz, S., Mettler-Altmann, T., and**
958 **Weber, A.P.M.** (2017). Photosynthesis in C_3-C_4 intermediate *Moricandia* species. J. Exp. Bot. **68**: 191–
959 206.
960 **Schlüter, U. and Weber, A.P.M.** (2020). Regulation and evolution of C_4 photosynthesis. *Annu. Rev. Plant Biol*.
961 **71**: 183–215.
962 **Schulze, S., Mallmann, J., Burscheidt, J., Koczor, M., Streubel, M., Bauwe, H., Gowik, U., and Westhoff,**
963 **P.** (2013). Evolution of C_4 photosynthesis in the genus *flaveria*: Establishment of a photorespiratory CO_2
964 pump. *Plant Cell* **25**: 2522–2535.
965 **Schulze, S., Westhoff, P., and Gowik, U.** (2016). Glycine decarboxylase in C_3, C_4 and C_3-C_4 intermediate
966 species. *Curr. Opin. Plant Biol*. **31**: 29–35.
967 **Sogbohossou, E.O.D., Achigan-Dako, E.G., Maundu, P., Solberg, S., Deguenon, E.M.S., Mumm, R.H.,**
968 **Hale, I., Van Deynze, A., and Schranz, M.E.** (2018). A roadmap for breeding orphan leafy vegetable
969 species: A case study of *Gynandropsis gynandra* (Cleomaceae). Hortic. Res. **5**: 2.
970 **Sogbohossou, E.O.D., Kortekaas, D., Achigan-Dako, E.G., Maundu, P., Stoilova, T., Van Deynze, A., de**
971 **Vos, R.C.H., and Schranz, M.E.** (2019). Association between vitamin content, plant morphology and
972 geographical origin in a worldwide collection of the orphan crop *Gynandropsis gynandra* (Cleomaceae).
973 *Planta* **250**: 933–947.
974 **Stamatakis, A.** (2014). RAxML version 8: A tool for phylogenetic analysis and post-analysis of large
975 phylogenies. *Bioinformatics* **30**: 1312–1313.
976 **Stanke, M., Steinkamp, R., Waack, S., and Morgenstern, B.** (2004). AUGUSTUS: A web server for gene
977 finding in eukaryotes. *Nucleic Acids Res*. **32**: W309–W312.
978 **Tu, X., Mejía-Guerra, M.K., Valdes Franco, J.A., Tzeng, D., Chu, P.Y., Shen, W., Wei, Y., Dai, X., Li, P.,**
979 **Buckler, E.S., and Zhong, S.** (2020). Reconstructing the maize leaf regulatory network using ChIP-seq
980 data of 104 transcription factors. *Nat. Commun*. **11**: 5089.
981 **Vaser, R., Sović, I., Nagarajan, N., and Šikić, M.** (2017). Fast and accurate *de novo* genome assembly from
982 long uncorrected reads. *Genome Res*. **27**: 737–746.

983 **Walker, B.J., Abeel, T., Shea, T., Priest, M., Abouelliel, A., Sakthikumar, S., Cuomo, C.A., Zeng, Q.,**
984 **Wortman, J., Young, S.K., and Earl, A.M.** (2014). Pilon: An integrated tool for comprehensive
985 microbial variant detection and genome assembly improvement. *PLoS One* **9**: e112963.
986 **Wang, D., Zhang, Y., Zhang, Z., Zhu, J., and Yu, J.** (2010). KaKs_Calculator 2.0: A Toolkit Incorporating
987 Gamma-Series Methods and Sliding Window Strategies. *Genomics, Proteomics Bioinforma*. **8**: 77–80.
988 **Wang, P., Vlad, D., and Langdale, J.A.** (2016). Finding the genes to build C_4 rice. *Curr. Opin. Plant Biol*. **31**:
989 44–50.
990 **Wang, X., Gowik, U., Tang, H., Bowers, J.E., Westhoff, P., and Paterson, A.H.** (2009). Comparative
991 genomic analysis of C_4 photosynthetic pathway evolution in grasses. *Genome Biol*. **10**: R68.
992 **Wang, Y., Chan, K.X., and Long, S.P.** (2021). Towards a dynamic photosynthesis model to guide yield
993 improvement in C_4 crops. *Plant J*. **107**: 343–359.
994 **Wang, Y., Tang, H., Debarry, J.D., Tan, X., Li, J., Wang, X., Lee, T.H., Jin, H., Marler, B., Guo, H.,**
995 **Kissinger, J.C., and Paterson, A.H.** (2012). MCScanX: A toolkit for detection and evolutionary analysis
996 of gene synteny and collinearity. *Nucleic Acids Res*. **40**: e49.
997 **Xu, Z. and Wang, H.** (2007). LTR-FINDER: An efficient tool for the prediction of full-length LTR
998 retrotransposons. *Nucleic Acids Res*. **35**: W265–W268.
999 **Yang, Z. et al.** (2020). A mini foxtail millet with an *Arabidopsis*-like life cycle as a C_4 model system. *Nat.*
1000 *Plants* **6**: 1167–1178.
1001 **Yang, Z.** (2007). PAML 4: Phylogenetic analysis by maximum likelihood. *Mol. Biol. Evol*. **24**: 1586–1591.
1002 **Zhao, H., Wang, Y., Lyu, M.-J.A., and Zhu, X.-G.** (2022). Two major metabolic factors for an efficient
1003 NADP-malic enzyme type C_4 photosynthesis. *Plant Physiol*. **189**: 84–98.
1004 **Zheng, Y. et al.** (2016). iTAK: A Program for Genome-wide Prediction and Classification of Plant
1005 Transcription Factors, Transcriptional Regulators, and Protein Kinases. *Mol. Plant* **9**: 1667–1670.
1006

Table 1 Global statistics of *G. gynandra* genome assembly and annotation

Genomic feature	Value
Genome assembly	
Estimated genome size	997.61 Mb
Assembled genome size (≥1,000 bp)	984.21 Mb
Assembled genome percentage	98.66%
GC content	39.20%
Total number of scaffolds	109
Scaffold N50	51.02 Mb
Longest scaffold	72.99 Mb
Total number of contigs	687
Contig N50	11.43 Mb
Longest contig	55.87 Mb
Sequence assigned to pseudochromosomes	909.61 Mb
Number of pseudochromosomes	17
Number of anchored and oriented contigs	171
Genome annotation	
Repetitive sequences	707.76 Mb
Repetitive sequences percentage	71.91%
Number of genes	34,772
Size of total gene length	119.12 Mb
Number of transcripts	41,843
Average length of transcripts	1,824 bp
Noncoding RNAs	12,441

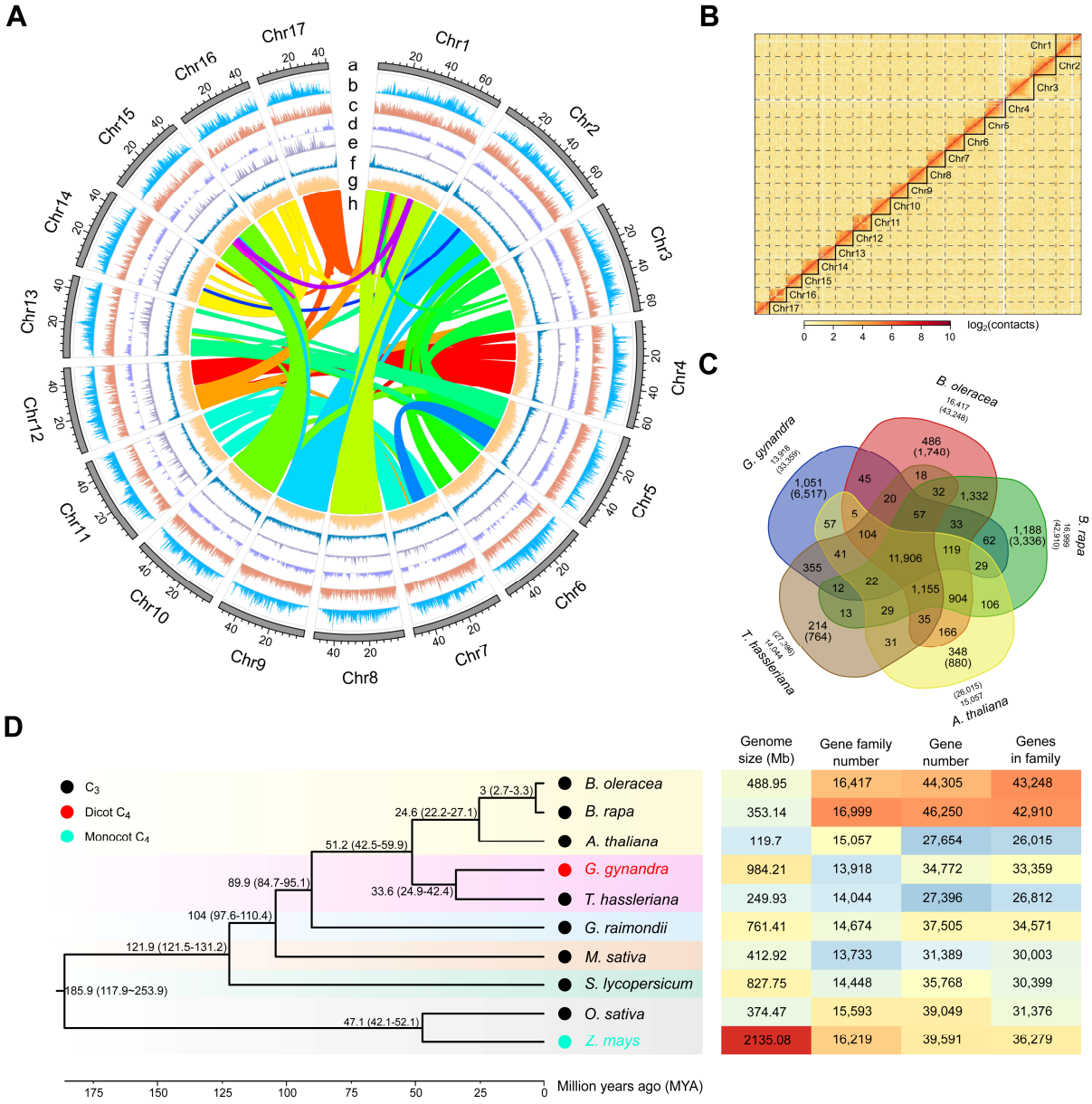

	Genome size (Mb)	Gene family number	Gene number	Genes in family
B. oleracea	488.95	16,417	44,305	43,248
B. rapa	353.14	16,999	46,250	42,910
A. thaliana	119.7	15,057	27,654	26,015
G. gynandra	984.21	13,918	34,772	33,359
T. hassleriana	249.93	14,044	27,396	26,812
G. raimondii	761.41	14,674	37,505	34,571
M. sativa	412.92	13,733	31,389	30,003
S. lycopersicum	827.75	14,448	35,768	30,399
O. sativa	374.47	15,593	39,049	31,376
Z. mays	2135.08	16,219	39,591	36,279

Figure 1 The high-quality assembly, genome features and evolutionary analysis of *G. gynandra*.

(A) An overview of the genomic characteristics of *G. gynandra*. The outermost annotations number successively the seventeen assembled chromosomes in descending order of size. Tracks from outer to inner circles depict length (Mb) of each chromosome (a), *Gypsy* retrotransposon distribution (b), *Copia* retrotransposon distribution (c), DNA transposon distribution (d), tandem repeats (e), gene density (f), GC content (g) and curve lines in the interior link the syntenic regions that have been retained presumably since the last whole-genome duplication event (h). Sliding window size is 200 kb.

(B) Genome-wide Hi-C heatmap of the *G. gynandra* genome. Heatmap shows the diagonal pattern for strong Hi-C interactions within intra-chromosome of *G. gynandra*. The X-axis and

Y-axis indicate the order positions of scaffolds on corresponding pseudo-chromosomes. The color bar denotes the interaction frequencies of the Hi-C links.

(C) Venn diagram illustrating the shared orthologous groups (orthogroups) among five species: *G. gynandra*, *T. hassleriana*, *B. rapa*, *B. oleracea* and *A. thaliana*. Each number represents the number of gene families shared among genomes. The number listed in parentheses is the total gene number among the orthogroups.

(D) Phylogenetic relationships of the two Cleomaceae and eight other species used in the study (*B. oleracea*, *B. rapa*, *A. thaliana*, *G. raimondii*, *M. sativa*, *S. lycopersicum*, *O. sativa* and *Z. mays*). The phylogenetic tree was constructed from single-copy orthologs of these species. Lineage divergence time is indicated at each branch point. The photosynthesis subtype of each species is marked by colored dots at each node. The genome size, gene family number, gene number and number of genes belonging to gene families for each species are listed in the heatmap at right.

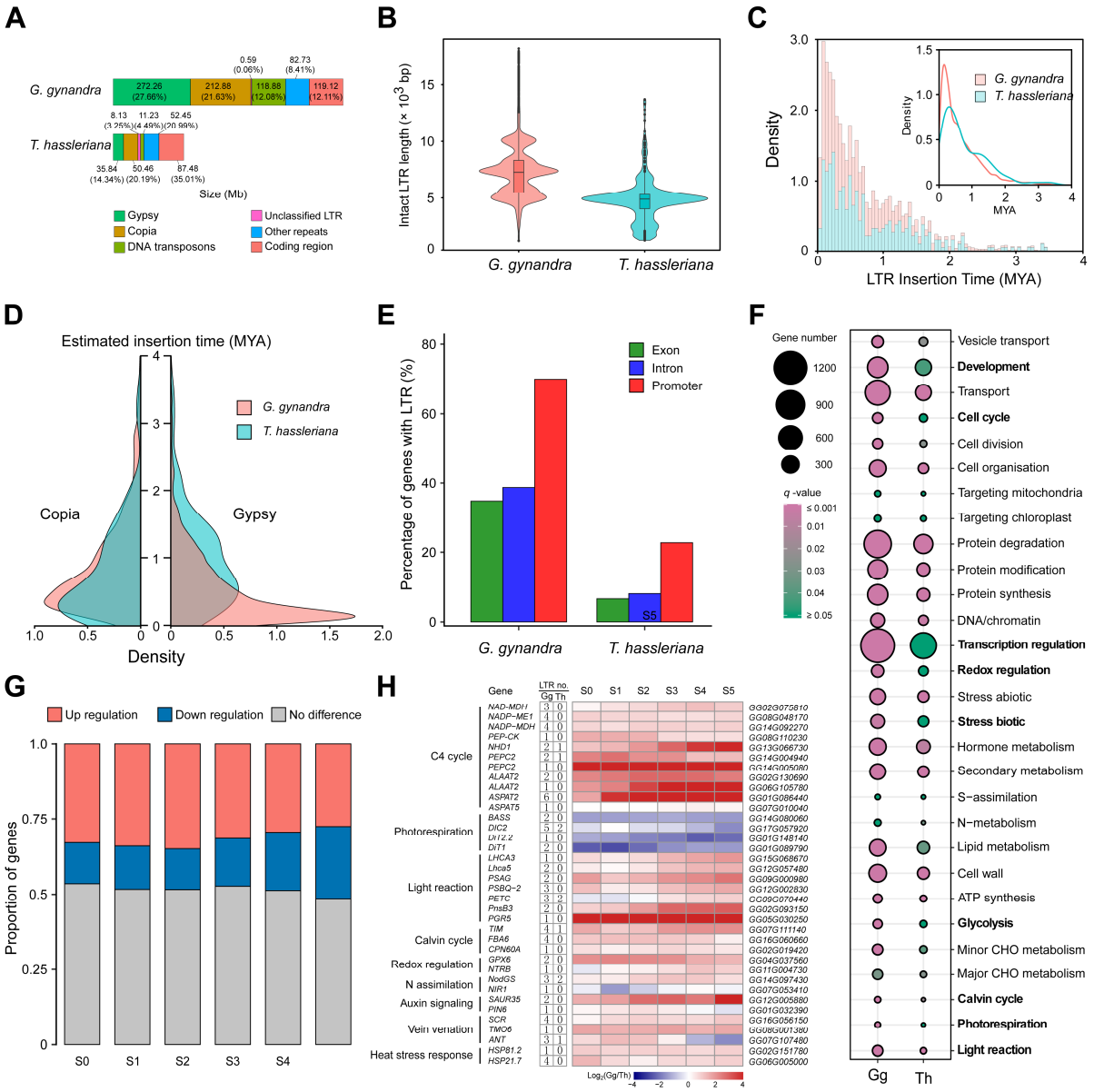

Figure 2 Comparative analysis of TEs in *G. gynandra* and *T. hassleriana* genomes, and the role of LTR-RTs in C_4 photosynthesis evolution.

(A) Genomic makeup by category of *G. gynandra* and *T. hassleriana.* The colored blocks indicate the sizes (Mb) of different components, including LTR-RTs (*Gypsy* and *Copia*), DNA transposons, unclassified LTR-RTs, other repeats and coding regions. The number in parentheses is the percentage each taking of the genome. Each number denotes the size (Mb) of each composition. *Gypsy*, *Copia* and DNA transposons were much more abundant in the *G. gynandra* genome than in *T. hassleriana*.

(B) Length distribution of intact LTR-RTs in *G. gynandra* and *T. hassleriana.* Boxes within violin plots indicate the first quartile, the median and the third quartile with whiskers extending up to 1.5× inter quartile range (IQR). Outliers are shown as dots, defined as data

points outside 1.5× IQR. The *G. gynandra* genome contained much more intact LTR-RTs of over 10 kb in length than *T. hassleriana*.

(C) Estimated insertion times of LTR-RTs into *G. gynandra* and *T. hassleriana* genomes. The X and Y axes indicate the insertion times and the density of intact LTR-RTs at each time, respectively. *G. gynandra* underwent more extensive LTR-RT explosion than *T. hassleriana* during the last 2 MYA.

(D) Temporal patterns of *Gypsy* and *Copia* bursts in *G. gynandra* as compared to *T. hassleriana*. The X-axis and Y-axis indicate the density of *Gypsy*/*Copia* and the insertion times, respectively. Despite *G. gynandra* and *T. hassleriana* shared similar density distributions of *Copia*, the former experienced a surge of *Gypsy* insertion very recently.

(E) Percentage of LTR-RT exon-, intron- or promoter-inserted genes. The 2 kb region upstream of the transcription start site is defined as the promoter region of gene. Genes with LTR-RT insertion in promoter regions are much more abundant than in exons or introns, especially in *G. gynandra*.

(F) MapMan-Bin enrichment of the LTR-RT promoter-inserted genes in *G. gynandra* and *T. hassleriana*. Annotations of protein sequences with MapMan terms were performed with the online Mercator (https://www.plabipd.de/portal/mercator4). The MapMan4 program was used to conduct the analysis, and the results were visualized with R software. The MapMan terms with clear differences between the two species are highlighted in bold.

(G) Histograms showing the proportion of selected LTR-RT promoter-inserted genes with up- or down-regulation in *G. gynandra* relative to *T. hassleriana*. The 6,283 genes, which have more LTR-RT insertions in their promoter regions in *G. gynandra* than in *T. hassleriana*, were used for expression analysis. This was performed with the previously deposited RNA-seq data of leaves at six developmental stages (from young to mature, S0 to S5) for these two *Cleome* species (Külahoglu et al., 2014). The gene expression levels were normalized with the upper quartile normalization procedure using the youngest S0 leaf stage of *G. gynandra* as the reference. No difference is defined if the levels of gene expression show lower than a 1.5 fold change between *G. gynandra* and *T. hassleriana*. The X-axis and Y-axis indicate leaf developmental stages and the proportion of genes in each regulation category, respectively. The proportions of up-regulated genes are overall higher than those down-regulated at all the analyzed leaf stages.

(H) Expression patterns of C_4 photosynthesis-related pathway genes that have more LTR-RT insertions in their promoter regions in *G. gynandra* than in *T. hassleriana*. Pathways and member genes are indicated at left. The two columns of numbers show how many LTR-RTs were found in the promoter region of each gene in *G. gynandra* and *T. hassleriana*, respectively. The right panel shows the ID of each gene copy in *G. gynandra*. The heatmap illustrates differential expression ratios of the genes between the two species at various leaf developmental stages (S0 to S5). Color reflects fold differences ($\log_2$ ratios) in gene expression. LTR no., number of LTR-RTs insertion.

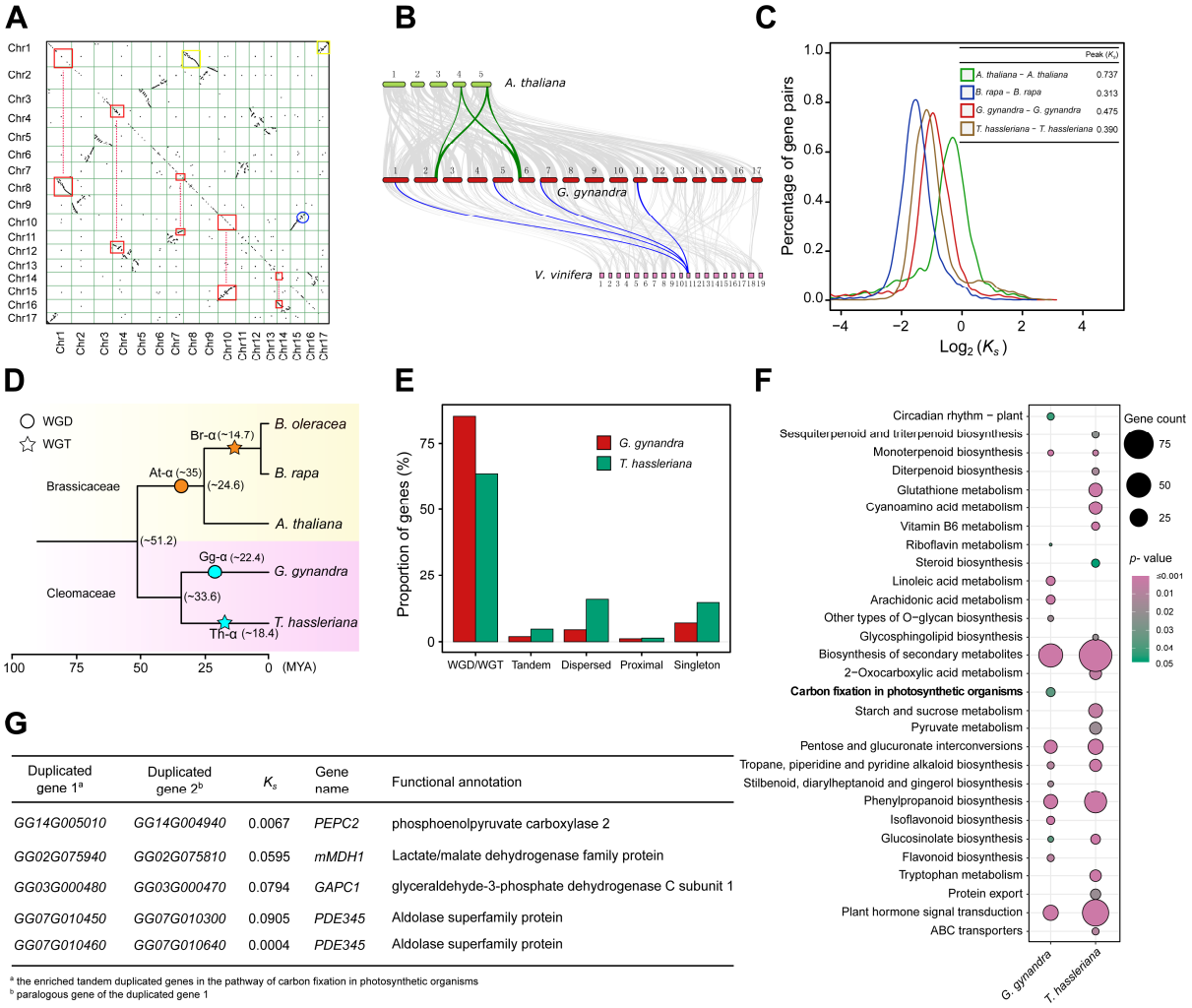

Duplicated gene 1[a]	Duplicated gene 2[b]	K_s	Gene name	Functional annotation
GG14G005010	*GG14G004940*	0.0067	*PEPC2*	phosphoenolpyruvate carboxylase 2
GG02G075940	*GG02G075810*	0.0595	*mMDH1*	Lactate/malate dehydrogenase family protein
GG03G000480	*GG03G000470*	0.0794	*GAPC1*	glyceraldehyde-3-phosphate dehydrogenase C subunit 1
GG07G010450	*GG07G010300*	0.0905	*PDE345*	Aldolase superfamily protein
GG07G010460	*GG07G010640*	0.0004	*PDE345*	Aldolase superfamily protein

[a] the enriched tandem duplicated genes in the pathway of carbon fixation in photosynthetic organisms
[b] paralogous gene of the duplicated gene 1

Figure 3 Analysis of WGD and tandem duplications in the *G. gynandra* genome.
(A) Dotplot figure showing syntenic duplicates within *G. gynandra* genome. The red squares linked by dash lines denote the extensive collinear relationships between chromosomes of *G. gynandra* due to the WGD event. The blue circle represents an intrachromosomal segment inversion. The big and small yellow boxes on Chr1 depict synteny with the chromosomes of Chr8 and Chr17, respectively, suggesting occurrence of potential chromosome breakage and fusion events following WGD.
(B) Micro-collinearity of *G. gynandra* genome with those of *A. thaliana* and *Vitis vinifera.* The parallel horizontal lines represent the chromosomes of *A. thaliana*, *G. gynandra* and *V. vinifera* genomes, with the connected grey ribbons indicating syntenic blocks. The 4-to-1 collinear relationship between *G. gynandra* and *V. vinifera* is highlighted by one syntenic set in blue, with one segment in *V. vinifera* traced to four regions in *G. gynandra*. The 2-to-2 collinear relationship between *G. gynandra* and *A. thaliana* is marked by two syntenic sets in green.
(C) K_s distribution of syntenic orthologs from *G. gynandra*, *T. hassleriana, A. thaliana* and *B. rapa.* The X and Y axis denotes $\log_2(K_s)$ and the percentage of gene pairs in the syntenic

blocks, respectively. The values of K_s peaks for each species are showed on the top right corner.

(D) The evolutionary relationship and paleo-polyploidization events in the five sequenced species of Brassicaceae and Cleomaceae. The paleo-polyploidization and time estimation are indicated on branches of the phylogenetic tree. The yellow and pink background colors represents the Brassicaceae and Cleomaceae families, respectively. The cyan circle and star highlight WGD (Gg-α) and WGT (Th-α) events in *G. gynandra* and *T. hassleriana*, respectively. The divergence time is listed in the brackets. The time scale (MYA) is shown at bottom.

(E) Gene duplication patterns in the genomes of *G. gynandra* and *T. hassleriana*. The graph indicates the proportion of genes classified by duplication mode relative to total genes of each species. The gene duplication modes were determined by MCScanX, including singletons, dispersed, proximal, tandem and WGD/WGT. WGD and WGT are the major modes of gene duplication for *G. gynandra* and *T. hassleriana*, respectively.

(F) KEGG enrichments of the tandem duplicated genes in *G. gynandra* and *T. hassleriana*. The size of the circle indicates enriched gene numbers in each pathway, with the color of the circle indicating enrichment *p*-value. Pathways with *p*-value < 0.05 are shown. The "carbon fixation in photosynthetic organisms" pathway is specifically enriched in *G. gynandra* (marked in bold).

(G) Tandem duplicated genes of the carbon fixation pathway enriched in *G. gynandra*. Duplicated gene paralogs are listed in columns 1–2. K_s values were calculated using the KaKs_Calculator for duplicated gene pairs (Wang et al., 2010). The K_s values of these genes were much lower than the K_s peak of Gg-α (0.475).

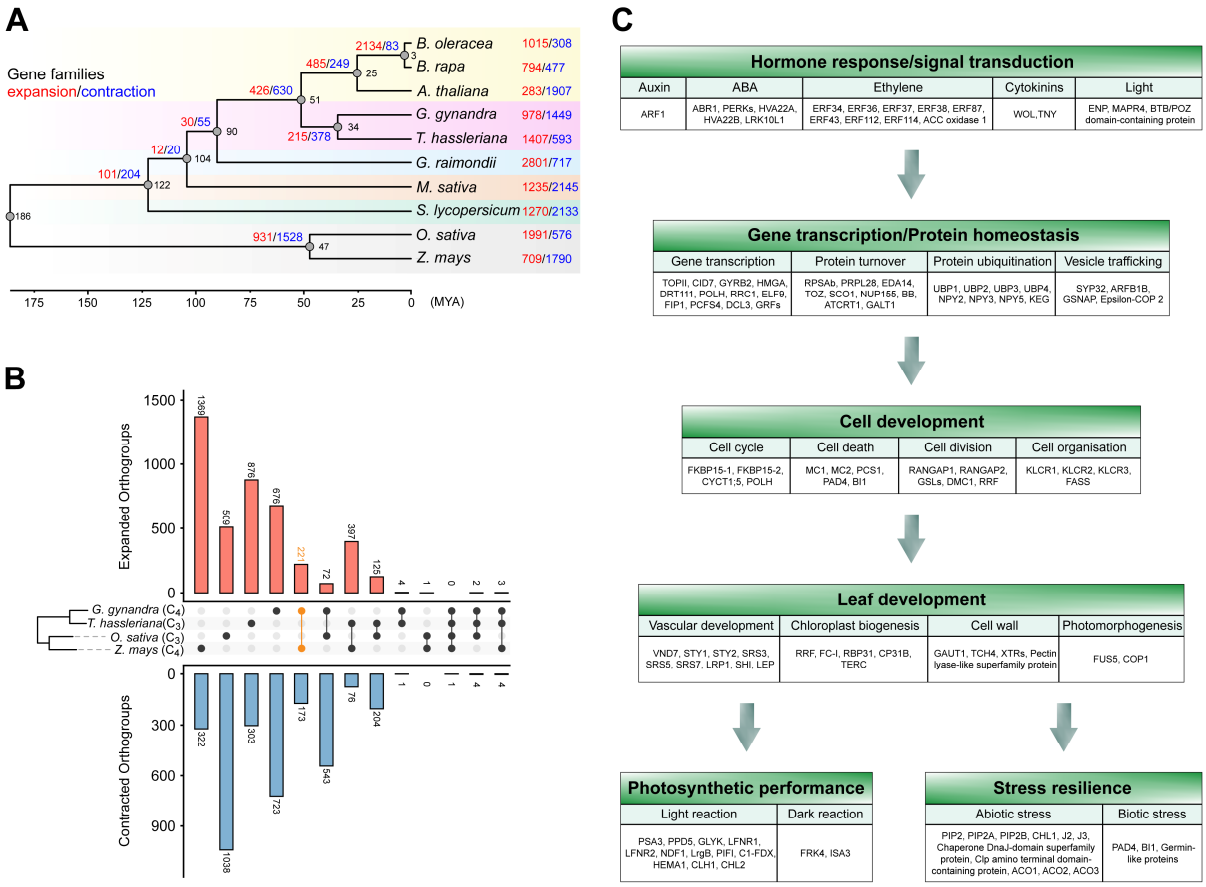

Figure 4 Analysis of gene family expansion and contraction in representative C_3 and C_4 plants.

(A) The number of gene families that expanded (red) or contracted (blue) during evolution mapped to the species phylogenetic tree. The black number at each node denotes the divergence time between the two branches. The time scale (MYA) is shown at bottom.

(B) Numbers of expanded and contracted orthogroups shared among the C_3 and C_4 lineages. The middle panels show phylogenetic tree and comparison groups of the four species, *G. gynandra* (C_4), *T. hassleriana* (C_3), *O. sativa* (C_3) and *Z. mays* (C_4). The upper and lower panels indicate the numbers of shared expanded and contracted orthogroups, respectively, with numbers noted for each bar. The number of expanded orthogroups shared between C_4 plants *G. gynandra* and *Z. mays* is marked in orange (221).

(C) Functional annotation of the expanded gene families common to *G. gynandra* and *Z. mays*. Arrows indicate biological processes potentially associated with the fitness advantages of C_4 plants, including hormone response/signal transduction, gene transcription/protein homeostasis, cell development, leaf development, photosynthetic performance and stress resilience. The genes within each biological process are divided into different categories based on their functional annotations from MapMan.

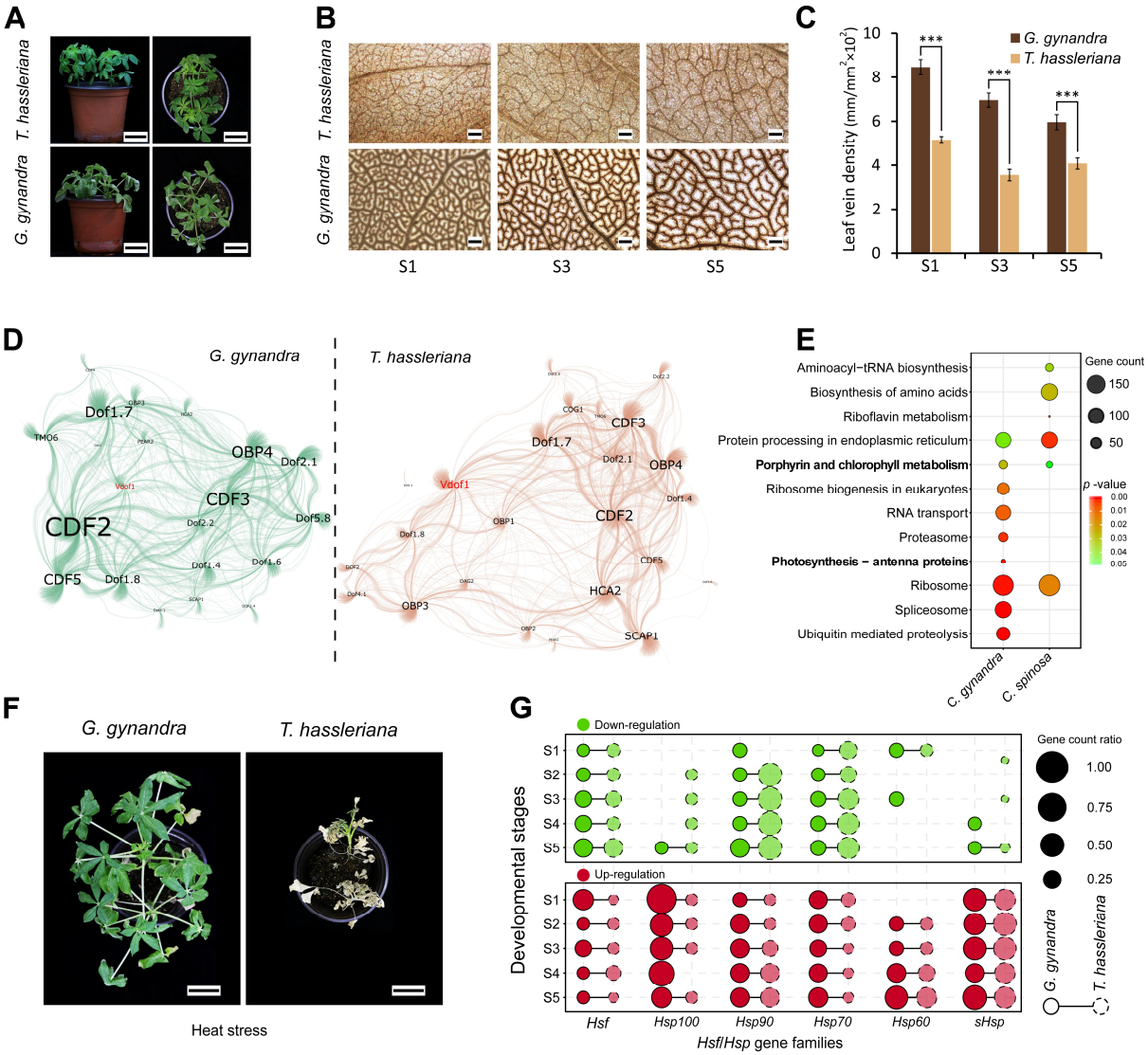

Figure 5 Higher leaf vein density and heat stress resistance in *G. gynandra* compared to *T. hassleriana* associated with gene expression modifications.

(A) The growth phenotype of *G. gynandra* (lower panel) and *T. hassleriana* (upper panel) under normal conditions. The photographs are taken from 5-week old plants. The left and right panels are side and top views, respectively. Scale bar = 5 cm.

(B) Overview of leaf vein patterns in *G. gynandra* (bottom) and *T. hassleriana* (top). Representative images from left to right illustrate vein density of the central region at leaf developmental stages from young to mature as numbered (S1, S3, S5). Scale bar = 200 µm.

(C) Analysis of the leaf vein density between *G. gynandra* and *T. hassleriana.* Vein density (vein length/area) for each leaf was assessed for six positions at a central region bounded by the midvein over three developmental stages. Student's *t* test (means ± SD; $n = 3$); ***$P < 0.001$.

(D) Networks of gene regulatory relationships between Dof transcription factors and their candidate target genes in *G. gynandra* and *T. hassleriana*. The gene regulatory networks (GRN) were constructed using GENIE3 and visualized with Gephi. The size of the labeled

hub gene names is based on the degree of connecting nodes. The edges of *G. gynandra* (left) and *T. hassleriana* (right) GRNs are indicated in green and tangerine colors, respectively. The *Vdof1* gene in the two GRNs is highlighted in red.

(E) KEGG pathway enrichment of the candidate target genes of the Vdof1 transcription factor in *G. gynandra* and *T. hassleriana*. The size of the circle indicates enriched gene numbers in each pathway, with the color of the circle indicating enrichment *p*-value. Pathways with *p*-value < 0.05 are shown. The photosynthesis-related pathways are marked in bold.

(F) *G. gynandra* displays exceptional tolerance to continuous high temperature stress compared with *T. hassleriana*. 5-week-old plants were subjected to heat treatments in a controlled growth chamber under conditions of 45/35 °C (16/8h) and 60% relative humidity for 15 days. Scale bar = 5 cm.

(G) The proportions of up- and down-regulated genes for *Hsf*/*Hsp* families after heat treatments in *G. gynandra* and *T. hassleriana*. The X-axis and Y-axis indicate *Hsf*/*Hsp* family names and different leaf developmental stages (from young to mature, S1 to S5), respectively. The size of the circle denotes the ratio of differentially expressed gene count relative to the total gene number of each *Hsf*/*Hsp* family. The lower (red) panel depicts the proportions of up-regulated genes, and the upper (green) panel shows the proportions of down-regulated genes.

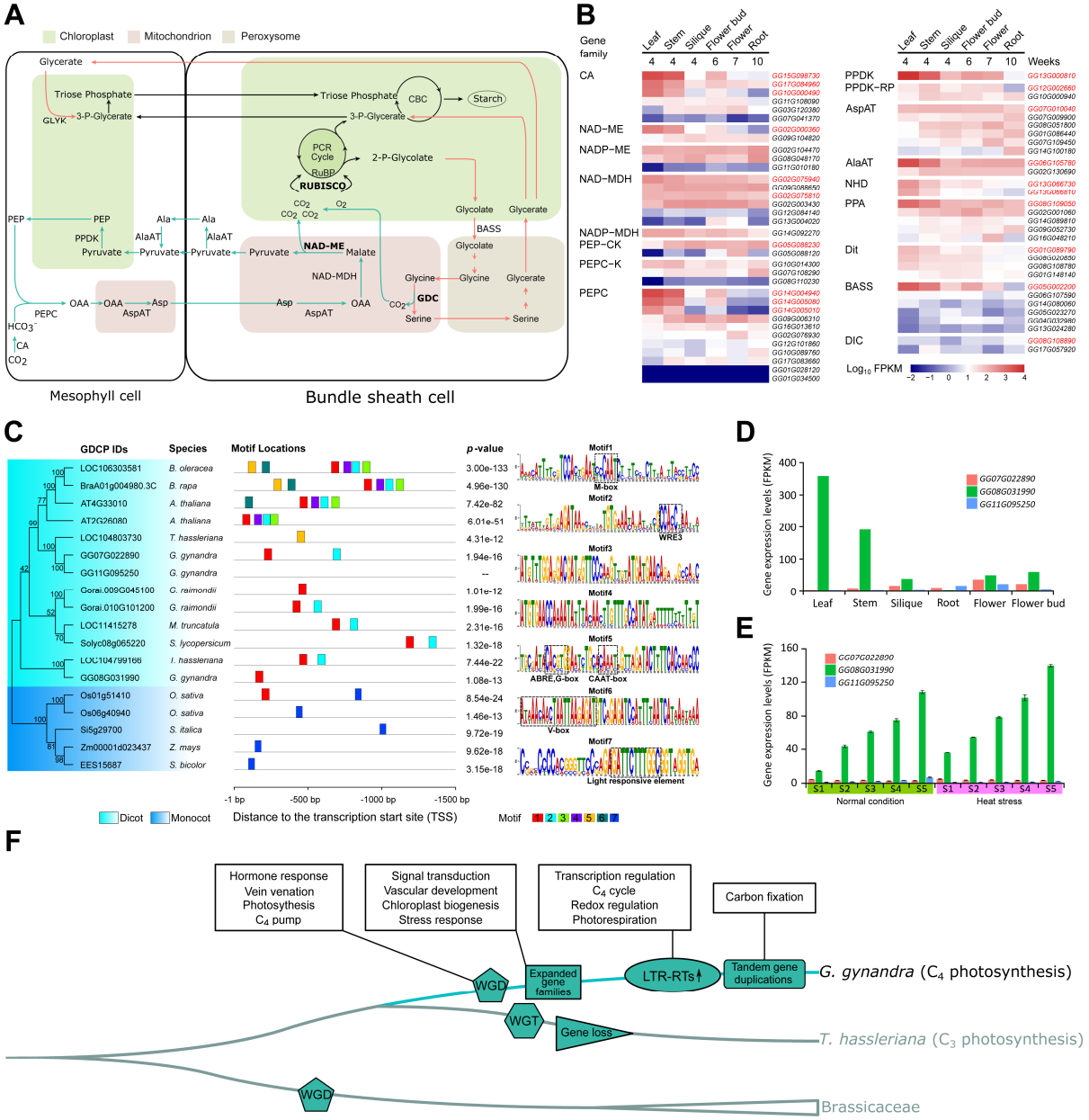

Figure 6 Evolution of C_4 photosynthesis in *G. gynandra*.

(A) Diagrammatic representation of main proteins and metabolic fluxes for the NAD-ME C_4 photosynthetic subtype in *G. gynandra*. Aspartate (Asp) converted from oxaloacetate (OAA) by AspAT in the mitochondria of mesophyll (M) cells is the main metabolite transported from M cells to BS cells. Asp is converted to OAA and then to malate (Mal), which is decarboxylated by NAD dependent malate dehydrogenase (NAD-MDH); Mal is further decarboxylated by NAD-ME, releasing CO_2 to the chloroplast of BS cells. The green arrows show the carbon dioxide (CO_2) accumulation pathway of NAD-ME subtype. Red arrows mark the photorespiratory pathway. The three key enzymes, RUBISCO, NAD-ME and GDC,

are in bold. Full names of metabolites and enzyme abbreviations are listed in Supplemental Data Set S21. PCR cycle, photosynthetic carbon reduction cycle; CBC, Calvin-Benson cycle.
(B) Heatmap showing the expression pattern of key genes involved in C_4 photosynthesis in photosynthetic and non-photosynthetic tissues of *G. gynandra*. The color denotes the expression level from low (blue) to high (red) expressed as $\log_{10}$FPKM. The ID of each gene copy in *G. gynandra* was indicated at right. The candidate C_4 genes for *G. gynandra* are highlighted in red.
(C) Phylogenetic tree and motifs in the promoter regions of *GDCP* genes in representative C_3 and C_4 plants. The left panel shows the phylogenetic tree of GDCPs, with light blue and dark blue backgrounds marking dicot and monocot species, respectively. The middle panel shows the type, location and *p*-values of conserved motifs in the upstream 1.5 kb regions from the transcription start site of each *GDCP* gene. The right panel shows the motif sequence and *cis*-acting regulatory elements highlighted by dashed boxes. The scale length (bp) and motif color key are shown at the bottom.
(D) The expression patterns of the three *GDCP* genes in different tissues of *G. gynandra*. Unique among the paralogs, *GG08G031990* gene showed very high level of expression in the leaf or stem.
(E) Analysis of expression levels of the three *GDCP* genes during *G. gynandra* leaf development under normal or heat stress conditions. The X-axis and Y-axis indicate gene expression level (FPKM) and leaf developmental stages (from young to mature, S1 to S5), respectively. Consistent with the results from Figure 6D, only *GG08G031990* was dominantly expressed in each stage analyzed, and its expression was even inducible by heat.
(F) A conceptual model reconstructing hypothesized key steps in the evolution and maintenance of C_4 photosynthesis in the spider plant. First, a recent whole-genome duplication (WGD, Gg-α) is the origin of C_4 pathway-related genes in *G. gynandra*, including genes involved in the hormone response, vein venation, C_4 metabolism, Calvin cycle, N and S assimilations and photorespiratory CO_2 pump. Second, expansions of defined gene families enable the establishment of C_4 features including signal transduction, vascular development, chloroplast biogenesis and stress response. Finally, more recent LTR-RT explosion and species-specific tandem duplications fine-tune the expression of C_4 photosynthesis-associated genes, including those involved in the light reaction, C_4 cycle, redox regulation and carbon fixation. While these steps can overlap and may not have taken place independently. The much higher leaf vein density and heat stress tolerance in *G. gynandra* compared to *T. hassleriana* are linked with shifted patterns of gene expression. Despite *T. hassleriana* underwent a whole-genome triplication (WGT, Th-α) event later than Gg-α, subsequent massive gene loss likely occurred, including missing the duplicated copies of certain C_4 metabolism genes. Besides, contrary to the photorespiration pathway, the overall expression levels of the C_4 pathway-related genes in *T. hassleriana* are markedly lower than in *G. gynandra*, which might have also constrained its evolution of C_4 photosynthesis.

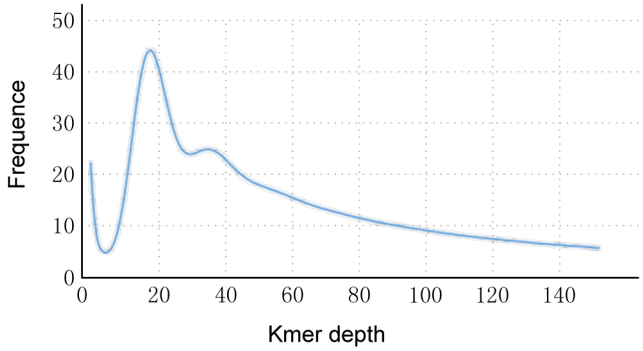

Supplemental Figure S1. Statistics for the frequencies and depths of 15 *k*-mers in the *G. gynandra* genome. The frequency indicates a bimodal curve caused by heterozygosity. X and Y axes show *k*-mer depth and frequency, respectively. Based on the formula Genome size = *k*-mer number/*k*-mer depth, the genome size of *G. gynandra* was measured to be 997.61 Mb.

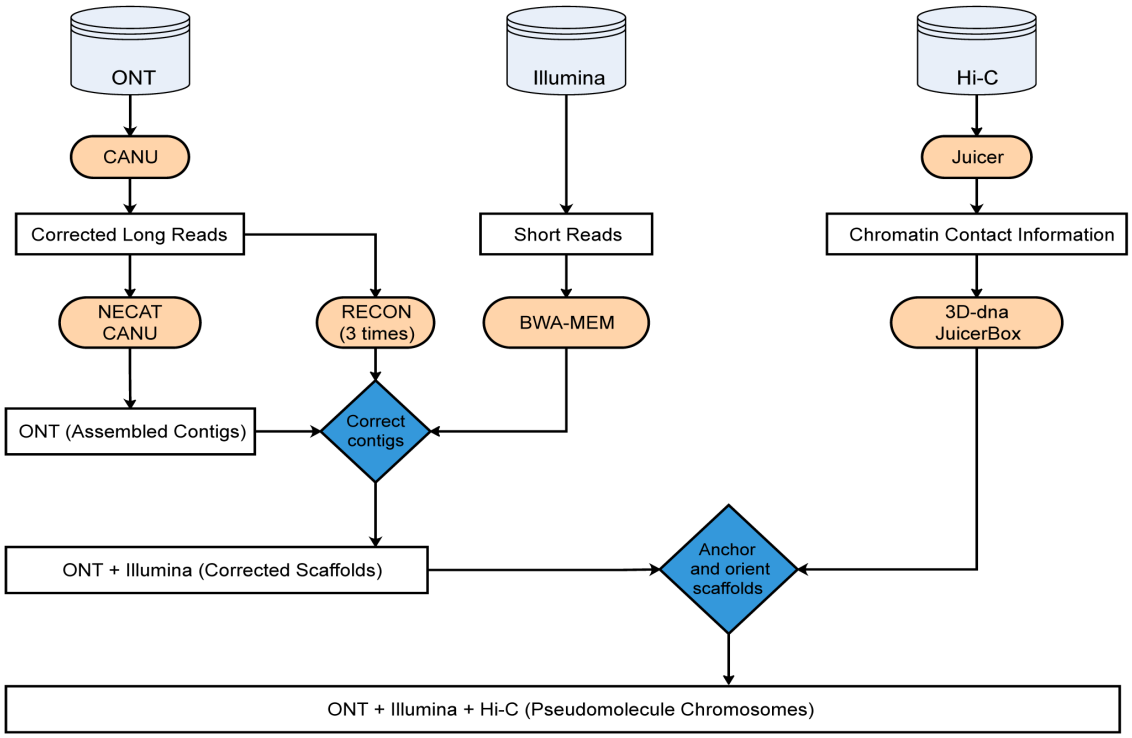

Supplemental Figure S2. Overview of the processing pipeline for assembling the *G. gynandra* genome. Three different datasets, Oxford Nanopore Technology (ONT) reads, Illumina short-reads and Hi-C mapping, were utilized for hybrid assembly strategy. ONT reads were used to performed contigs assembly. Subsequently, the ONT reads and Illumina short reads were used to correct these scaffolds, and Hi-C mapping was used to anchor and orient the scaffolds into pseudomolecule chromosomes.

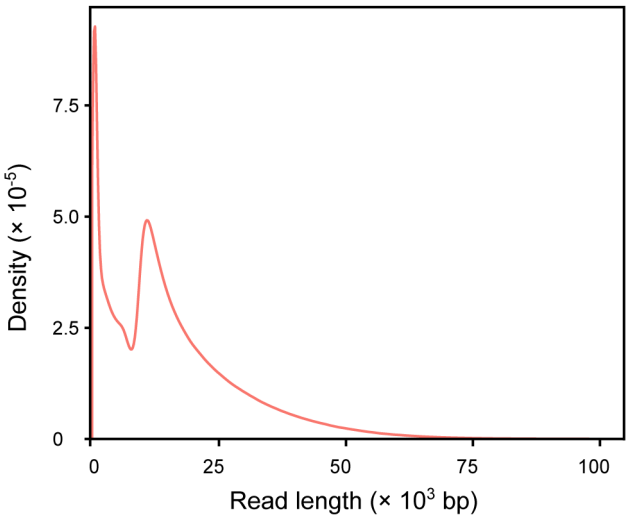

Supplemental Figure S3. Length distribution of ONT sequencing reads. The X axis and Y axis show length and frequency, respectively.

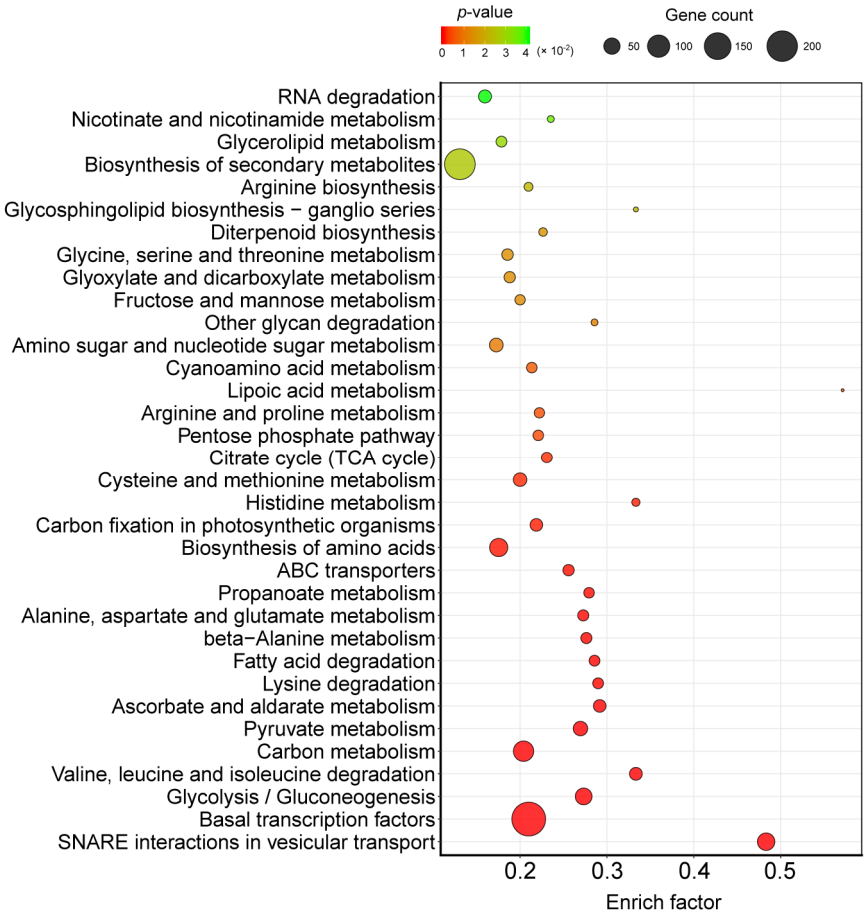

Supplemental Figure S4. KEGG functional enrichment analysis of gene families specific to *G. gynandra*. The size of the circle indicates enriched gene number of pathway. The color of the circle indicates the enrichment *p*-value of pathway. The significant cutoff for the enrichments was set as *p*-value < 0.05.

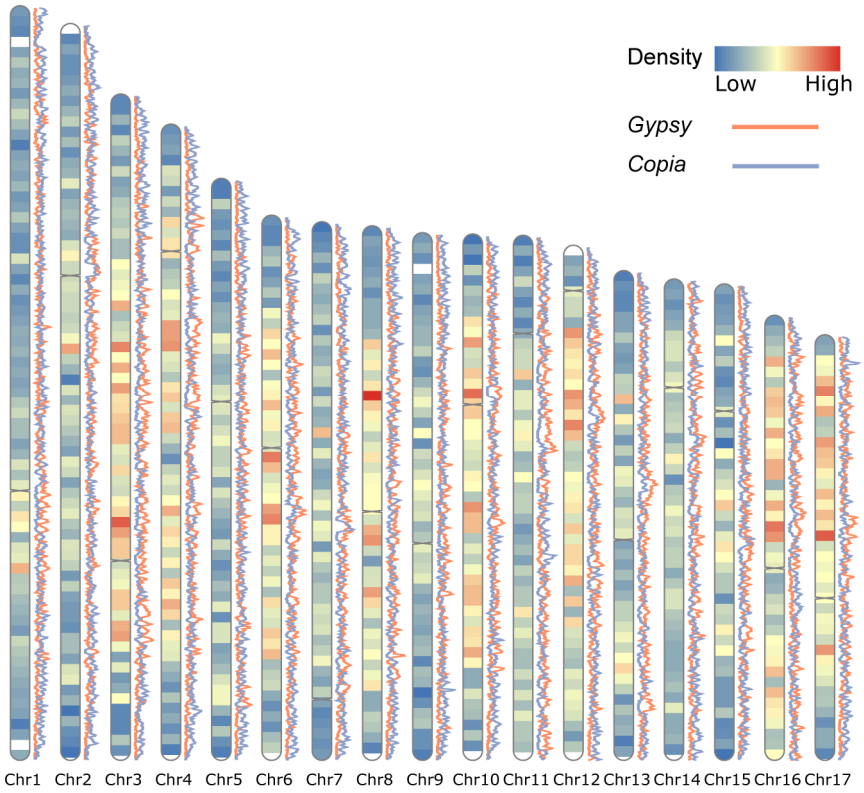

Supplemental Figure S5. The density distribution of intact LTRs, *Gypsy* and *Copia* in each chromosome of *G. gynandra*. The window size was 100 kb for *Gypsy* and *Copia*, and 1 Mb for intact LTRs. The color from blue to red on the bar density scale indicates a density of LTR-RTs from low to high. These data were visualized using the R package RIdeogram.

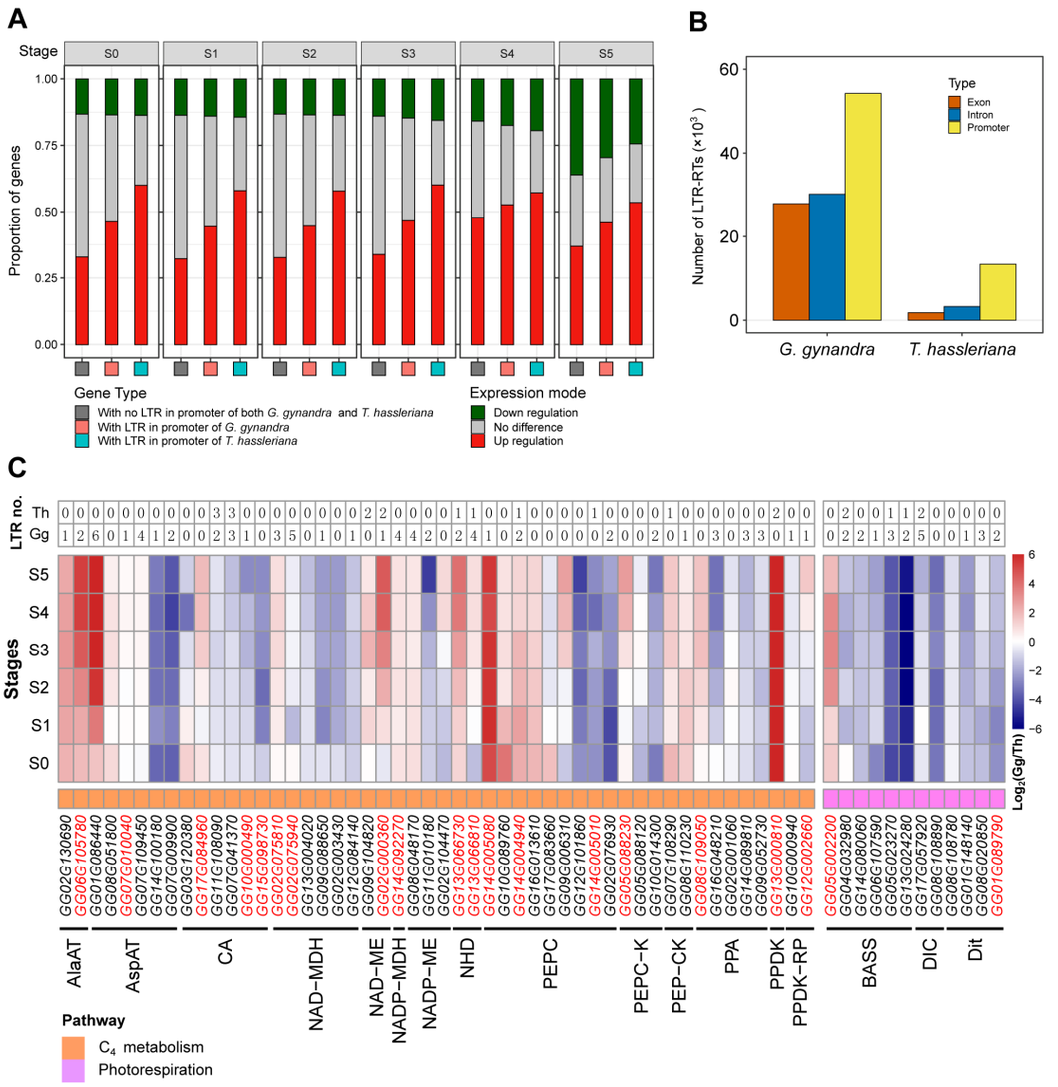

Supplemental Figure S6. Genomic distribution of LTR-RTs and their impacts on expression patterns of the C_4 pathway-associated genes in *G. gynandra* compared to *T. hassleriana*. (A) Histograms showing effects of absence or presence of LTR-RT insertions on the gene expression patterns in *G. gynandra* compared to *T. hassleriana*. The 20,094 homologous gene pairs identified between *G. gynandra* and *T. hassleriana* were used for expression analysis. The genes were classed into three groups including genes with no LTR-RT in promoters of both *G. gynandra* and *T. hassleriana* (dark grey), genes with LTR-RT only in promoters of *G. gynandra* (pink), and genes with LTR-RT only in promoters of *T. hassleriana* (blue). The analysis was performed with RNA-seq data of leaves at six developmental stages (from young to mature, S0 to S5) for these two *Cleome* species (Figure 2G). The gene expression levels were normalized with the upper quartile normalization procedure using the youngest S0 leaf stage of *G. gynandra* as the reference. No difference (light grey) is defined if the levels of gene expression show lower than a 1.5 fold change between *G. gynandra* and *T. hassleriana*. The X-axis and Y-axis indicate leaf developmental stages and the proportion of genes in each regulation category, respectively. **(B)** Numbers of LTR-RTs inserted in exon, intron and promoter regions of the *G. gynandra* or *T. hassleriana* genome. The 2 kb region upstream of the transcription start site (TSS) was designated as the promoter region of gene. Much more of LTR-RTs insertion in promoter regions than exons or introns seen both in *G. gynandra* and *T. hassleriana*. **(C)** Expression patterns of the C_4 pathway-related genes with altered number of LTR-RTs in *G. gynandra* relative to *T. hassleriana*. The gene names and gene IDs are showed at left and right, respectively. The two columns of numbers show how many LTR-RTs were found in the promoter region of each gene in *G. gynandra* and *T. hassleriana*, respectively. The right panel shows the ID of each gene copy in *G. gynandra*. The heatmap depicts differential expression ratios of the genes between the two species at various leaf developmental stages (S0 to S5). Color reflects fold differences ($\log_2$ ratios) in gene expression. The pathways of C_4 circle (orange) and photorespiration (magenta) are indicated beside the heatmap. LTR no., number of LTR-RTs insertion.

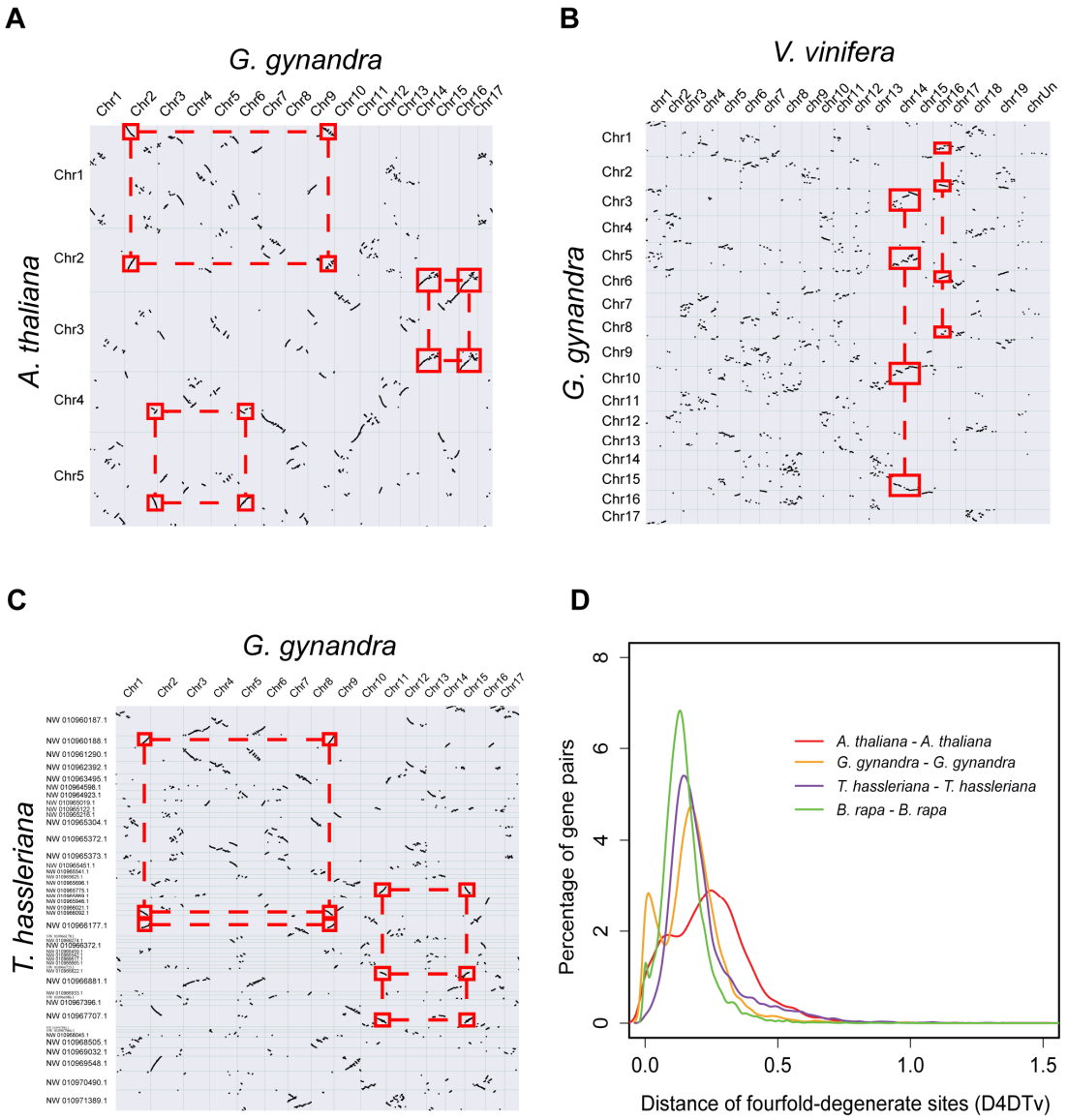

Supplemental Figure S7. Comparative genomic analysis of the WGD event in *G. gynandra*. (A) Syntenic dot plot in *G. gynandra* versus *A. thaliana* genome comparison. The red squares linked by dash lines indicate the synteny blocks between the two genomes. The collinear relationship of 2-to-2 is showed between *G. gynandra* and *A. thaliana*. **(B)** Dotplot figure of the collinear blocks between *V. vinifera* and *G. gynandra* genomes. The red squares linked by dash lines indicate the synteny blocks between the two genomes. The collinear relationship of 4-to-1 is showed between *G. gynandra* and *V. vinifera*. **(C)** Dotplot figure showing the collinear blocks between *G. gynandra* and *T. hassleriana* genomes. Listed are the 45 largest scaffolds of the genome assembly against the 17 *G. gynandra* chromosomes. The red squares linked by dash lines indicate the synteny blocks between the two genomes. The collinear relationship of 3-to-2 is showed between *G. gynandra* and *T. hassleriana*. **(D)** Distribution of 4DTv distance between syntenic orthologous genes within *A. thaliana*, *G. gynandra*, *T. hassleriana* and *B. rapa*. The X axis and Y axis show 4DTv values and the percentage of gene pairs in the syntenic blocks, respectively.

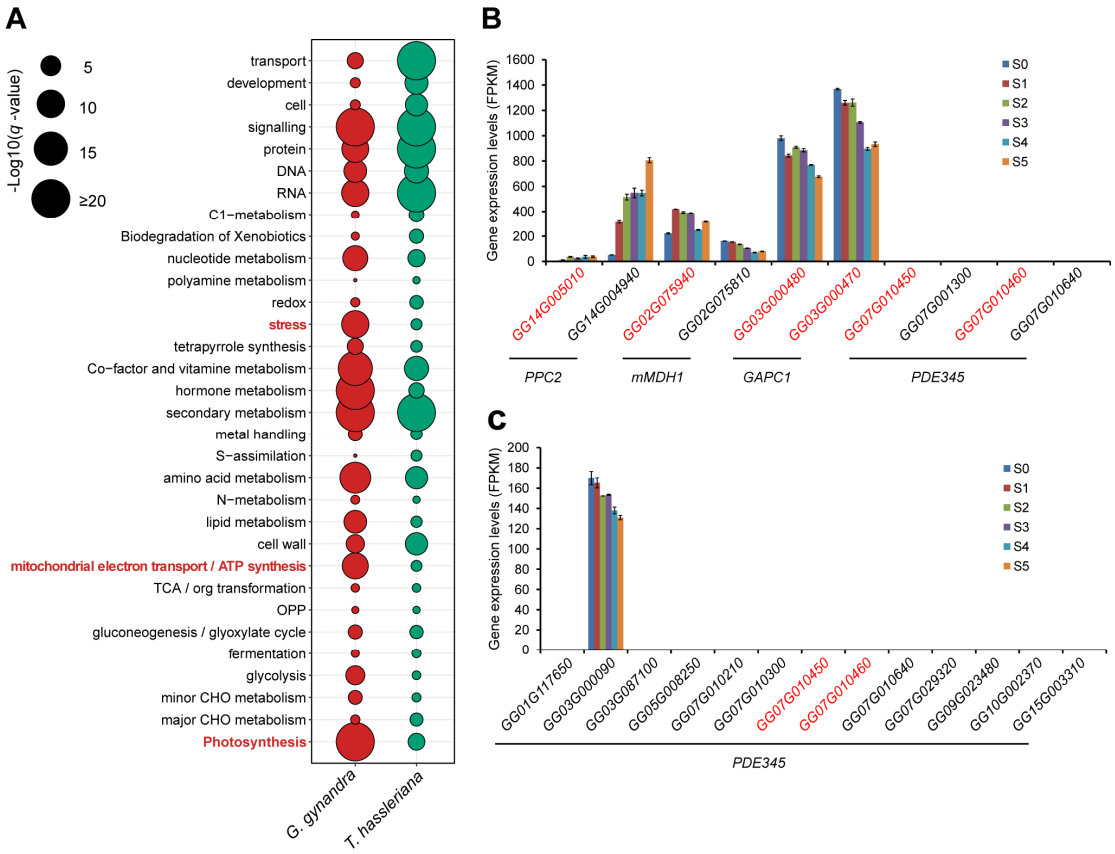

Supplemental Figure S8. Functional enrichment of WGD-derived genes and expression analysis of TD-derived genes in *G. gynandra*. (A) MapMan-Bin enrichment analysis of WGD-derived genes in *G. gynandra* and WGT-derived genes in *T. hassleriana*. The annotation of *G. gynandra* and *T. hassleriana* protein sequences with MapMan terms was performed with the online Mercator (https://www.plabipd.de/portal/mercator4). MapMan4 program was used to conduct MapMan-Bin enrichment analysis for the WGD/WGT-derived genes of the two Cleome species. The size of the circle represents $-\log_{10}(q\text{-value})$ of pathway enrichment. The distinctive MapMan terms in *G. gynandra* as compared to *T. hassleriana* were marked in red bold font. **(B)** Altered gene expression patterns of the carbon fixation pathway in photosynthetic organisms along leaf development gradients for *G. gynandra*. Histograms showing expression levels of the tandem duplicated genes (red) and their paralogues (black). Except for the *PDE345* gene, all the other tandem duplicated genes and their paralogues were differentially expressed in leaves of different developmental stages (from young to mature, S0 to S5). The gene expression analysis was performed as described in Figure 2G. **(C)** Histograms showing expression levels of all the duplicated copies of *PDE345* gene. Note that only one copy of the *PDE345* (*GG03G000090*) was expressed and the tandem duplicated ones (*GG07G010450* and *GG07G010460*) were also not.

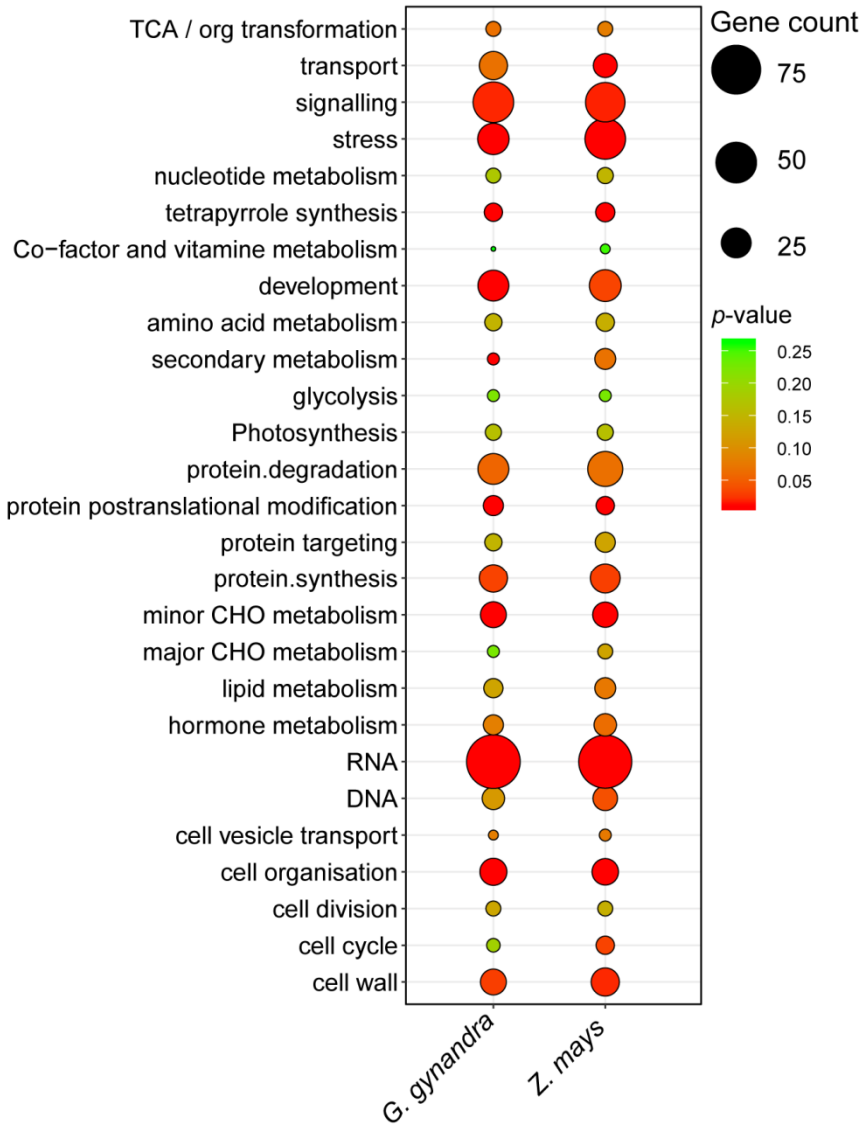

Supplemental Figure S9. MapMan-Bin enrichment analysis of 221 expanded gene families common to *G. gynandra* and *Z. mays*. The color and size of the circle indicate *p*-value and enriched gene number of pathway, respectively.

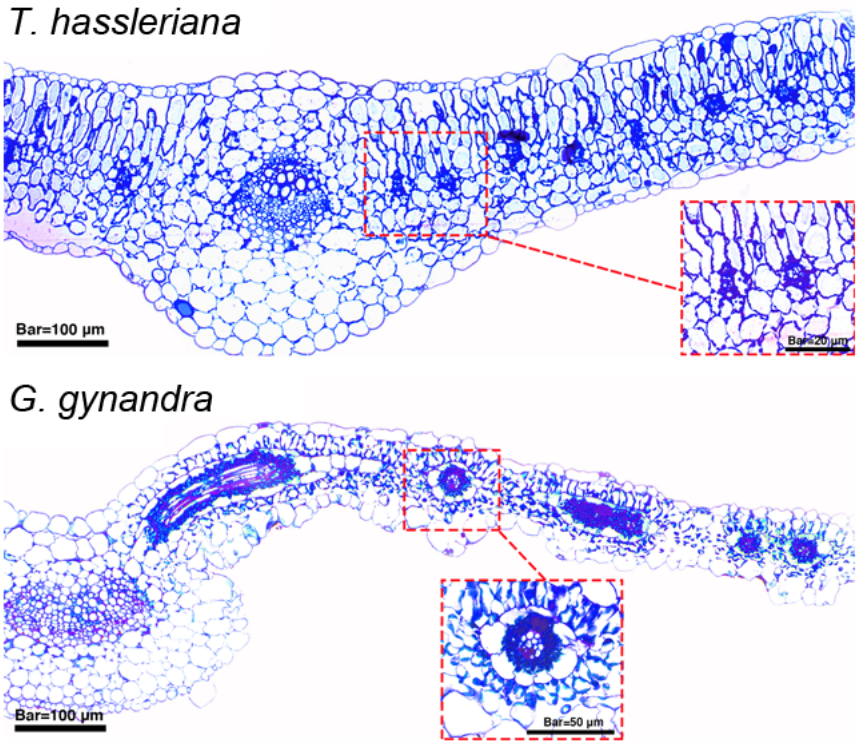

Supplemental Figure S10. Representative anatomy of the leaf cross-section of *G. gynandra* and *T. hassleriana*. The red dotted boxes indicate the cross-sectional area of bundle sheath (BS) cells.

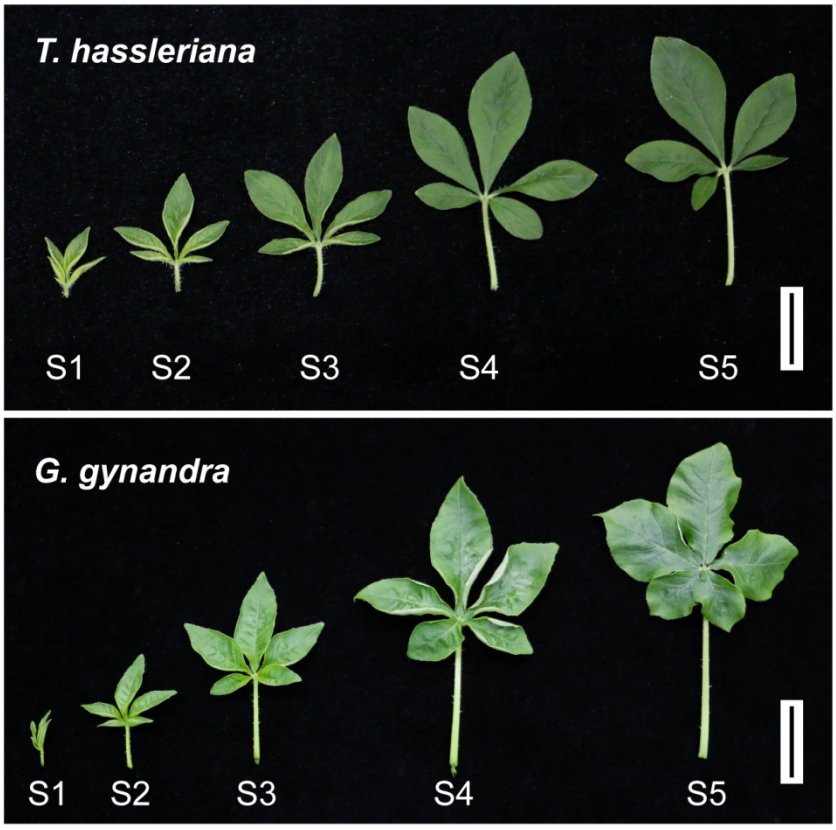

Supplemental Figure S11. The morphology of leaves at different developmental stages for *G. gynandra* and *T. hassleriana*. Images of leaves from left to right represent stages of 1, 2, 3, 4 and 5 from young to mature for the 5-week-old plants. Bars = 3 cm.

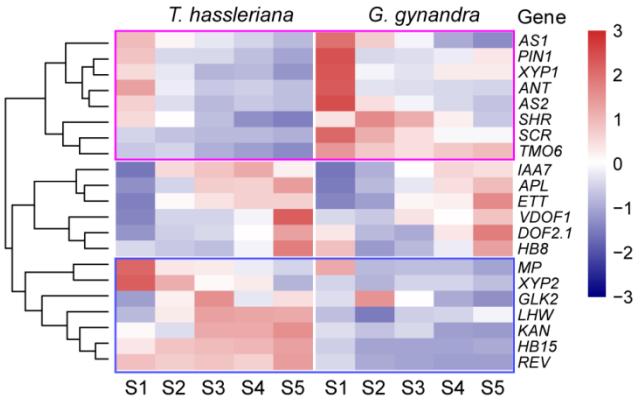

Supplemental Figure S12. The expression patterns of leaf and vasculature-related regulatory genes along leaf development gradients for *G. gynandra* and *T. hassleriana*. The red box represented the up-regulated genes, while the blue box represented the down-regulated genes in *G. gynandra* as compared to *T. hassleriana* (from young to mature, S1 to S5).

G. gynandra

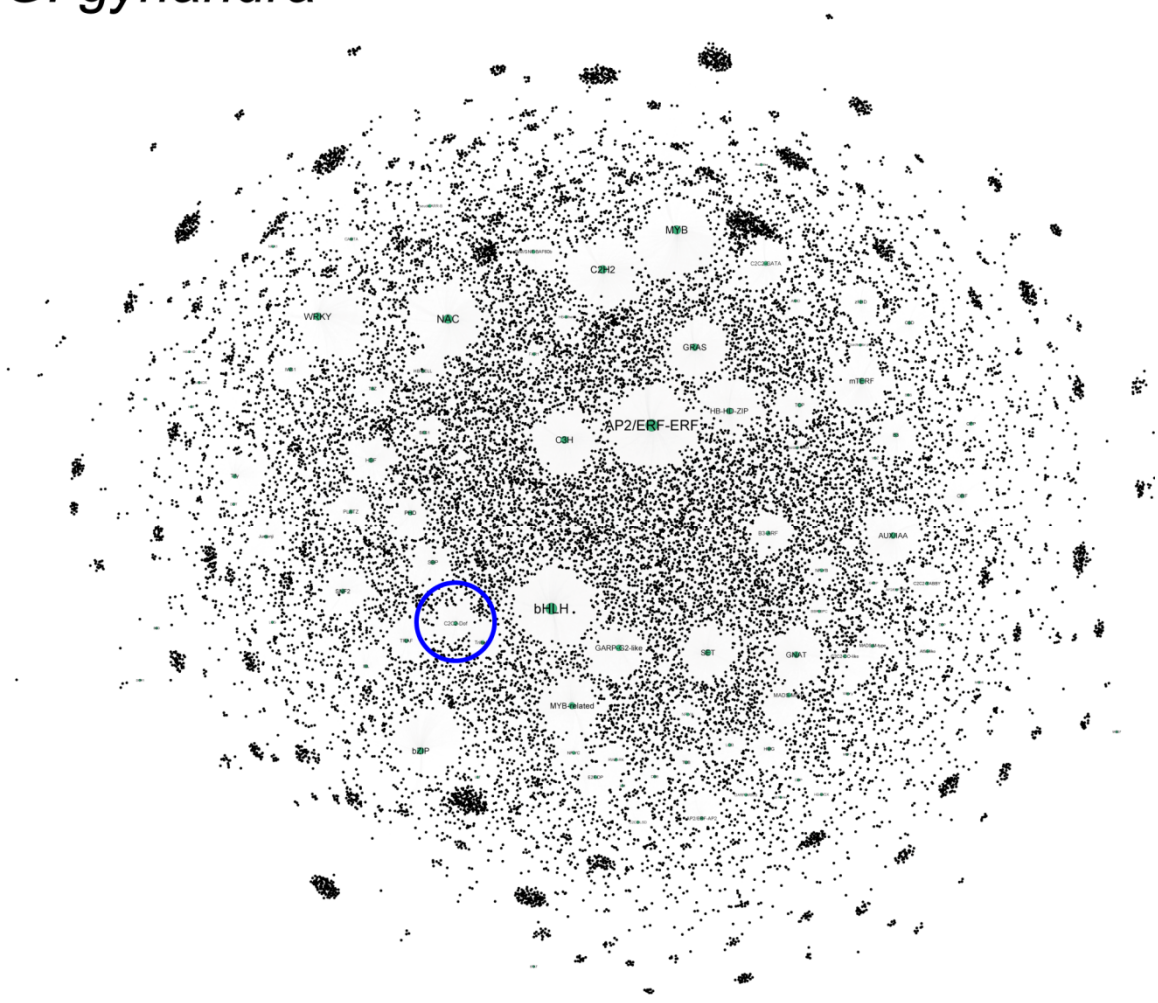

T. hassleriana

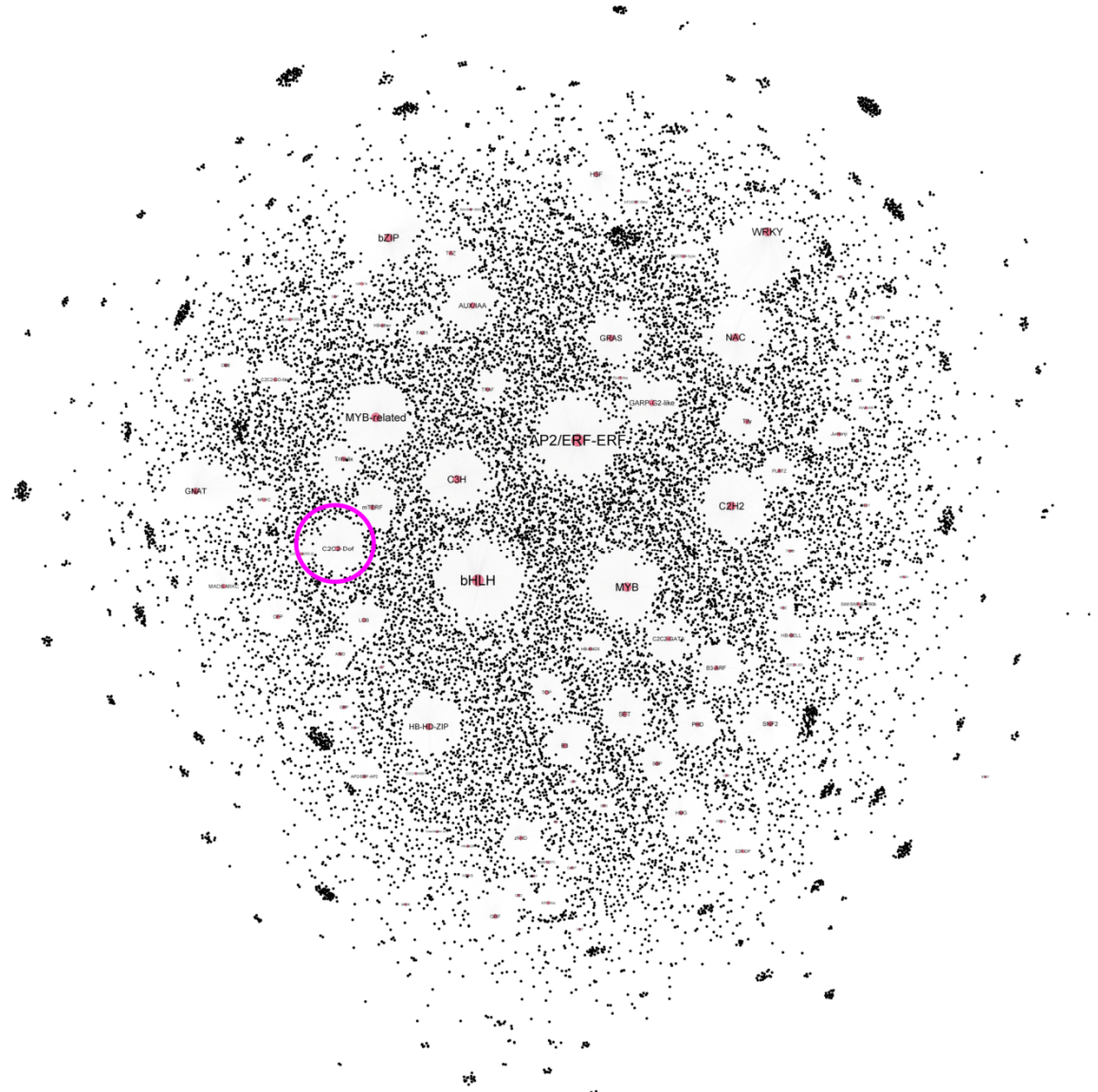

Supplemental Figure S13. The gene regulatory networks (GRNs) between transcription factors and their candidate target genes in *G. gynandra* or *T. hassleriana*. GRNs were constructed using GENIE3 based on the expression levels of genes during the development of leaves. The networks were visualized with Gephi. The size of the labeled hub genes was proportional to the degree of interconnected nodes. The green and red dots represented the TF families of *G. gynandra* and *T. hassleriana*, respectively. The *Dof* families were highlighted by blue and pink circles in the GRNs of *G. gynandra* and *T. hassleriana*, respectively.

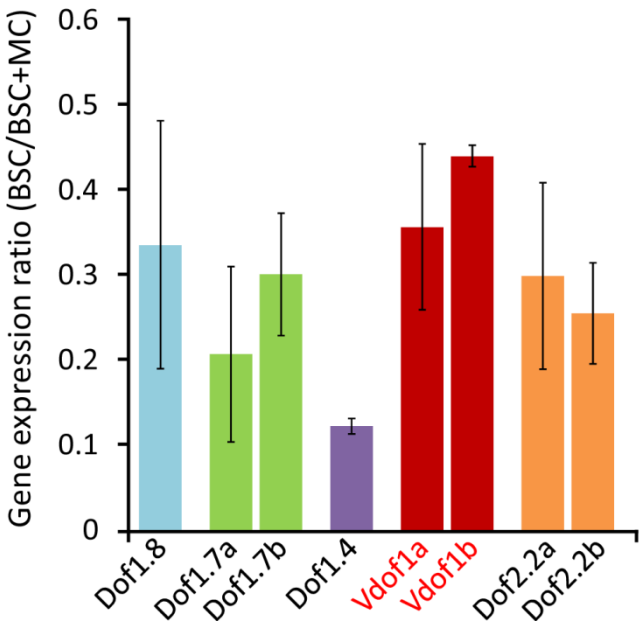

Supplemental Figure S14. Enrichment of *Vdof1* gene in leaf BS cells. *G. gynandra* has two homologous genes for *Vdof1* (*Vdof1a* and *Vdof1b*; highlighted in red). BSC, bundle sheath (BS) cells; MC, mesophyll (M) cells.

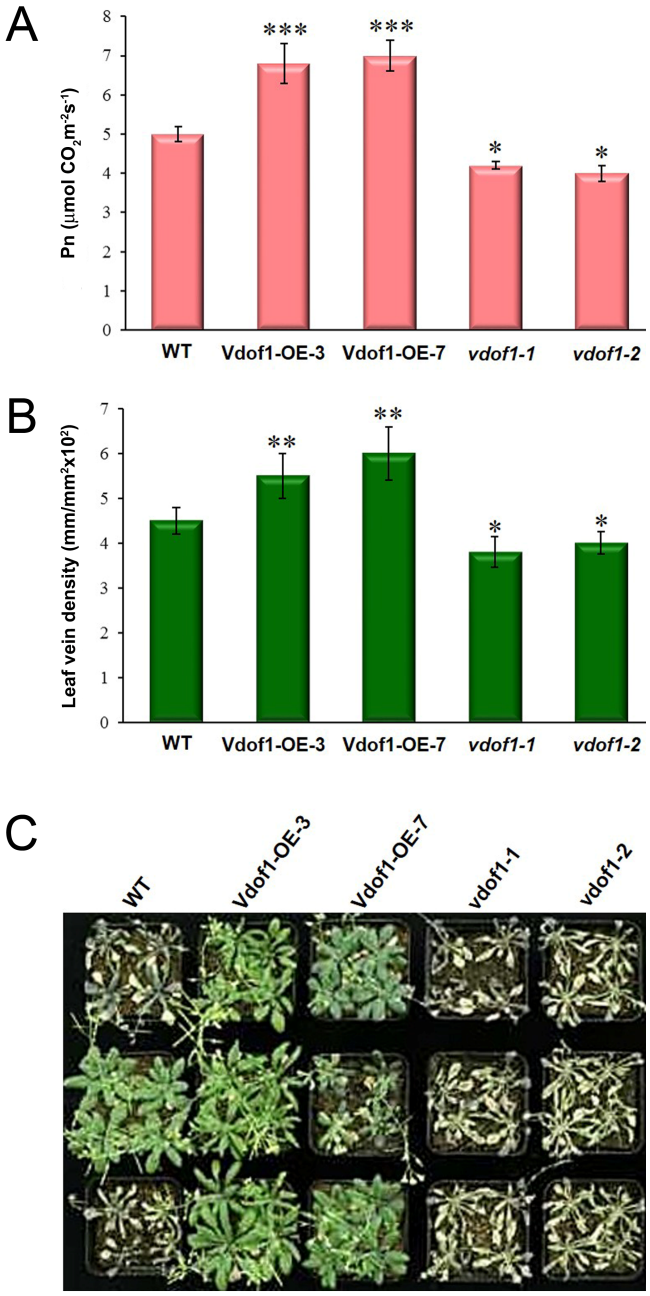

Supplemental Figure S15. Overexpression of *Vdof1* gene led to enhanced photosynthetic capacity, leaf vein density and tolerance to heat stress. (A) Analysis of rates of leaf photosynthetic carbon assimilation (Pn) in *Arabidopsis* wild type (WT), *Vdof1* (*AT4G24060*) overexpression lines (OE) and *vdof1* mutants (*vdof1-1*, SALK152104; *vdof1-2*, SAIL554A02). **(B)** Analysis of leaf vein density in *Arabidopsis* WT, *Vdof1* overexpression lines and *vdof1* mutants. Student's *t* test (means ± SD; $n = 3$); $*P < 0.05$; $**P < 0.01$; $***P < 0.001$. **(C)** Phenotypes of *Arabidopsis* WT, *Vdof1* overexpression lines and *vdof1* mutants subjected to heat stress. 5-week-old plants were treated with high temperature of 45 °C for two days and then shifted to normal conditions allowing recovery for additional two days.

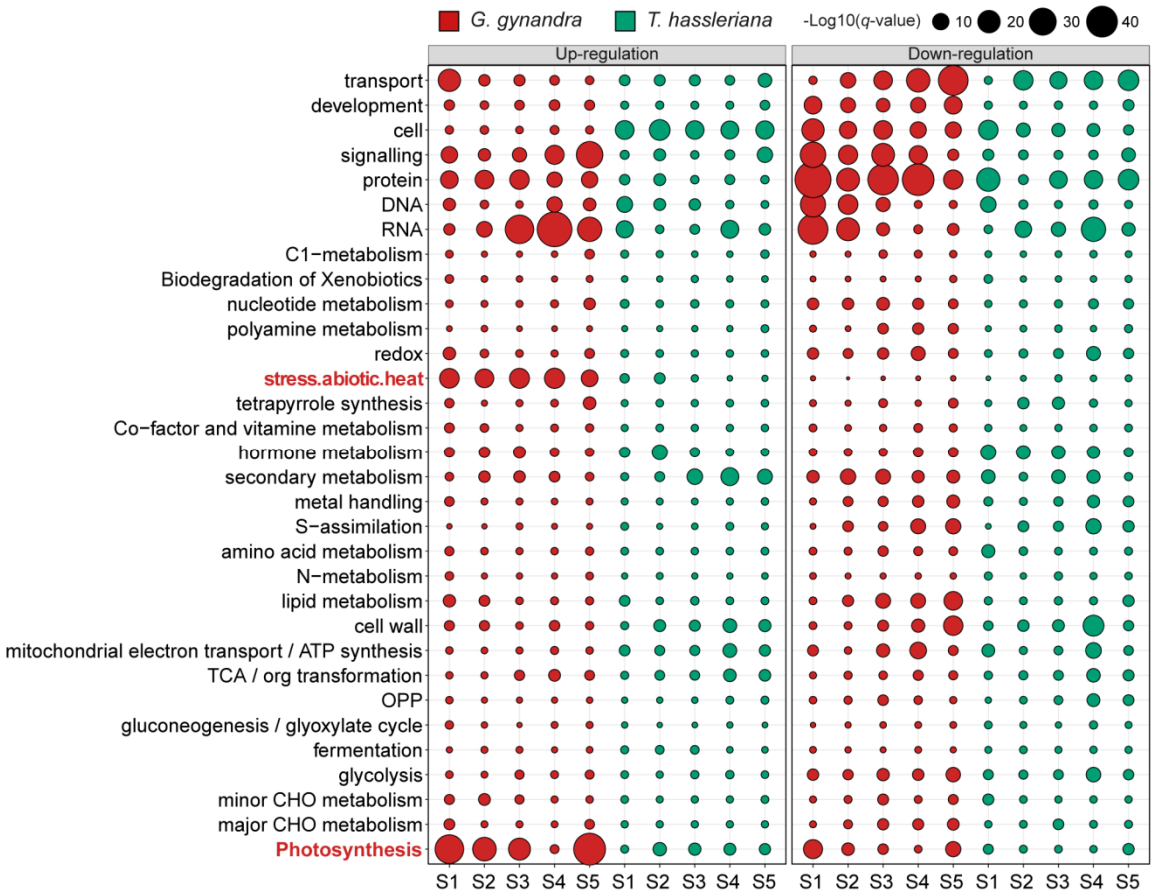

Supplemental Figure S16. MapMan-Bin enrichment analysis of DEGs at different stages of leaves from *G. gynandra* and *T. hassleriana* subjected to heat stress. The X axis and Y axis indicate leaf developmental stages (from young to mature, S1 to S5) and pathways, respectively. The sizes of the circle indicate -$\log_{10}$(*q*-value) of pathway enrichment. The red and green represent *G. gynandra* and *T. hassleriana*, respectively. The left and right panels show the enrichments of up-regulated and down-regulated genes, respectively. The significantly up-regulated pathways in *G. gynandra* relative to *T. hassleriana* were highlighted by red bold font.

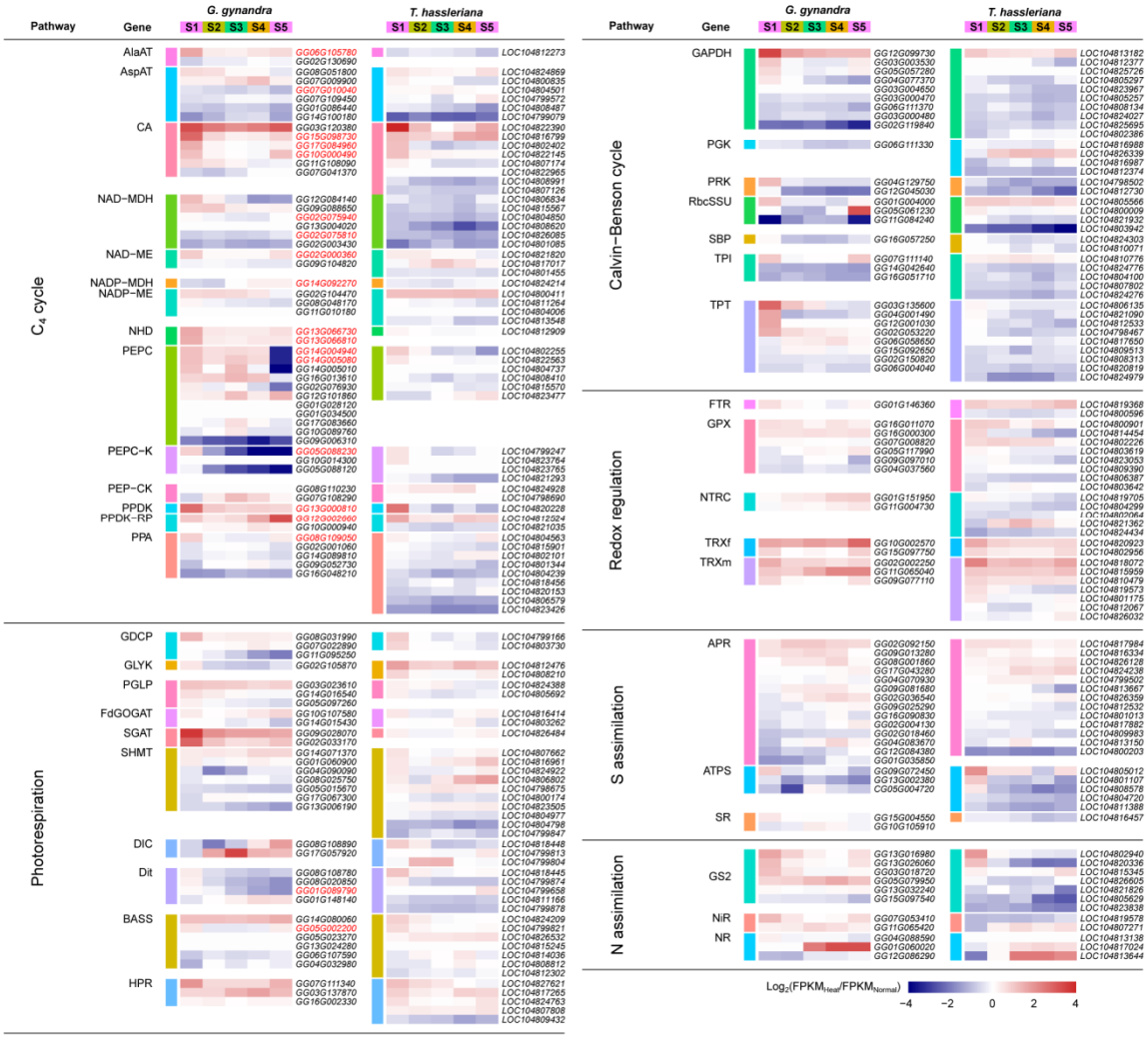

Supplemental Figure S17. Heatmap showing expression patterns of C_4 photosynthesis-related pathway genes under heat stress in *G. gynandra* and *T. hassleriana*. Pathways and member genes are indicated at left. The gene IDs are marked at right. The heatmaps show differential expression ratios of the genes after heat treatments at various leaf developmental stages (from young to mature, S1 to S5) within the two species. The color denotes fold differences ($\log_2$ ratios) in gene expression. FPKM: fragments per kb per million mapped reads.

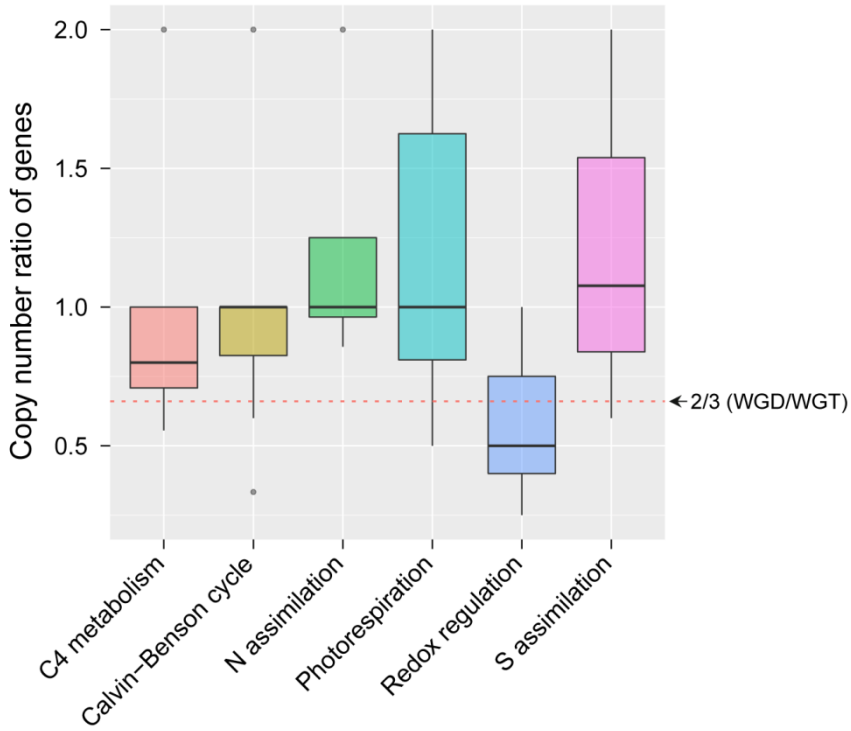

Supplemental Figure S18. Copy number ratio of genes for C_4 photosynthesis-related pathways in *G. gynandra* as compared to *T. hassleriana*. The red dash line indicates the expected theoretical 2-to-3 relationship for *G. gynandra* (WGD event) versus *T. hassleriana* (WGT event).

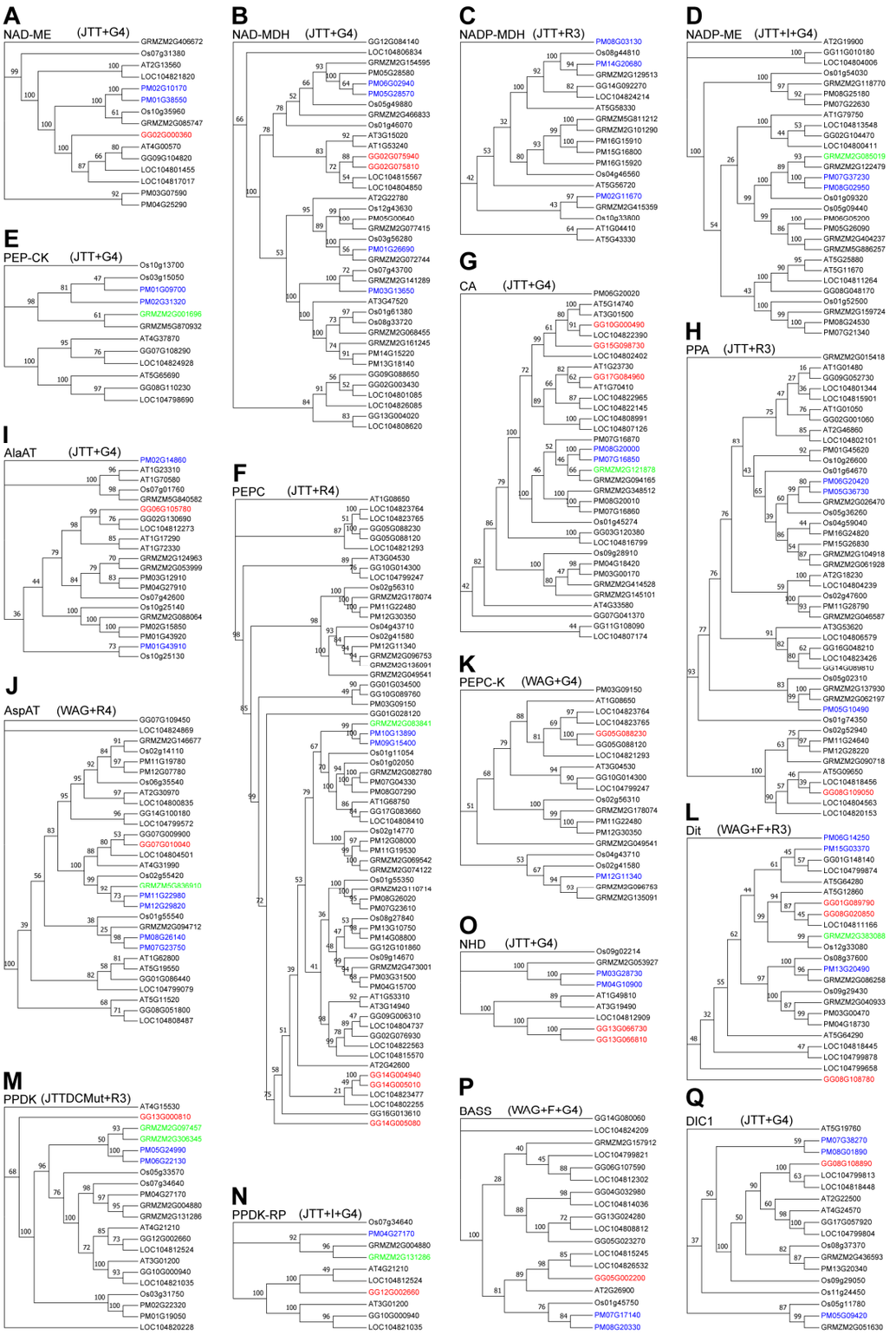

Supplemental Figure S19. Phylogenetic trees of C_4 photosynthesis-related genes. NAD-ME **(A)**, NAD-MDH **(B)**, NADP-MDH **(C)**, NADP-ME **(D)**, PEP-CK **(E)**, PEPC **(F)**, CA **(G)**, PPA **(H)**, AlaAT **(I)**, AspAT **(J)**, PEPC-K **(K)**, Dit **(L)**, PPDK **(M)**, PPDK-RP **(N)**, NHD **(O)**, BASS **(P)** and DIC1 **(Q)**. Maximum-likelihood gene trees were reconstructed from multiple protein sequence alignment using IQ-TREE. Numbers at each branch point indicate the percentage of supports from 1000 bootstraps. The best-fit evolutionary model of each tree is showed in the parentheses beside each gene name. Candidate C_4 genes from *G. gynandra* are in red fonts. Genes from different plant species are distinguished by the leading letters of the accession. Os - rice, PM - *Panicum miliaceum*, GRMZM - maize, GG - *G. gynandra*, LOC - *T. hassleriana*, AT - *A. thaliana*.

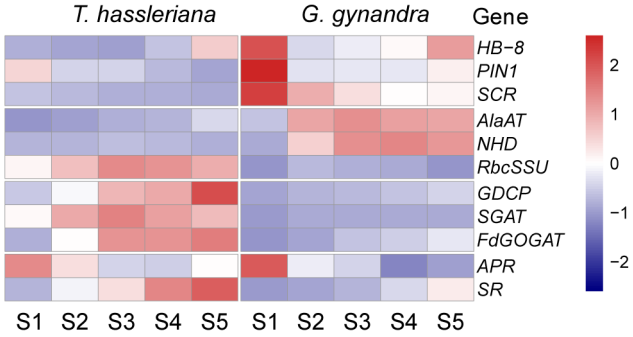

Supplemental Figure S20. The expression levels of C_4 pathway-related genes with lower copy numbers in *T. hassleriana* than in *G. gynandra* along leaf development gradients. S1 to S5 represented the different developmental stages of leaf from young to mature. The color from blue to red on the color bar scale indicates a normalized gene expression level from low to high.